Bayesian Pseudo-Coresets via Contrastive Divergence

Piyush Tiwary[1] **Kumar Shubham**[1] **Vivek V. Kashyap**[1] **Prathosh A.P.**[1]

[1]Department of Electrical Communuication Engineering,
Indian Institute of Science, Bengaluru, Karnataka 560012, India

Abstract

Bayesian methods provide an elegant framework for estimating parameter posteriors and quantification of uncertainty associated with probabilistic models. However, they often suffer from slow inference times. To address this challenge, Bayesian Pseudo-Coresets (BPC) have emerged as a promising solution. BPC methods aim to create a small synthetic dataset, known as pseudo-coresets, that approximates the posterior inference achieved with the original dataset. This approximation is achieved by optimizing a divergence measure between the true posterior and the pseudo-coreset posterior. Various divergence measures have been proposed for constructing pseudo-coresets, with forward Kullback-Leibler (KL) divergence being the most successful. However, using forward KL divergence necessitates sampling from the pseudo-coreset posterior, often accomplished through approximate Gaussian variational distributions. Alternatively, one could employ Markov Chain Monte Carlo (MCMC) methods for sampling, but this becomes challenging in high-dimensional parameter spaces due to slow mixing. In this study, we introduce a novel approach for constructing pseudo-coresets by utilizing contrastive divergence. Importantly, optimizing contrastive divergence eliminates the need for approximations in the pseudo-coreset construction process. Furthermore, it enables the use of finite-step MCMC methods, alleviating the requirement for extensive mixing to reach a stationary distribution. To validate our method's effectiveness, we conduct extensive experiments on multiple datasets, demonstrating its superiority over existing BPC techniques. Our implementation is available at https://github.com/backpropagator/BPC-CD

1 INTRODUCTION

In recent years, contemporary deep learning models have demonstrated exceptional effectiveness in a wide array of applications, spanning computer vision, natural language processing, and speech analysis [Krizhevsky et al., 2017b, Devlin et al., 2018, Amodei et al., 2016, He et al., 2016a, Dosovitskiy et al., 2020, Radford et al., 2021]. Conventional deep learning methods rely on one-time training of models providing point estimates [Szegedy et al., 2013]. These point estimates are prone to overfitting and often provide overconfident or under-confident outputs [Gawlikowski et al., 2023, Kabir et al., 2018]. This prohibits the use of deep learning models in critical applications such as medical, finance, etc [Ker et al., 2017, Cavalcante et al., 2016]. Bayesian methods furnish a systematic framework for parameter estimation and quantification of associated uncertainty. Bayesian inference entails sampling from parameter posterior distributions using Markov Chain Monte Carlo (MCMC) techniques [Robert et al., 1999, Robert and Casella, 2011]. However, conducting inference based on parameter posterior conditioned on the entire dataset is computationally demanding, particularly as the dataset size, denoted by N, increases. The computational complexity of MCMC methods scales with N as $\Theta(NS)$, where S denotes the number of samples [Campbell and Broderick, 2018]. This complexity becomes prohibitively high for large N. To mitigate this, one often resorts to using a random subset of $M \ll N$ data points for likelihood computation at each iteration [Bardenet et al., 2017, Korattikara et al., 2014, Maclaurin and Adams, 2014, Welling and Teh, 2011, Ahn et al., 2012, Bierkens et al., 2019, Pollock et al., 2020]. However, such approximations introduce errors and lead to slow mixing of Markov chains [Johndrow et al., 2020, Nagapetyan et al., 2017, Betancourt, 2015].

Bayesian coresets [Huggins et al., 2016] were introduced to solve the aforementioned problem. Particularly, Huggins et al. [2016] proposed to select a subset of original dataset (also called a coreset) that uniformly approximates the log-likelihood of the original dataset. These coresets are significantly smaller in size than the original dataset, leading to vastly improved sampling efficiency. Further, Campbell and Beronov [2019] proposed to identify the coreset by minimizing Kullback-Leibler (KL) divergence between full data posterior and coreset posterior. However, most of such methods do not scale with data dimension [Manousakas et al., 2020]. Particularly, the KL-divergence between the (optimal) coreset posterior and true posterior increases with data dimension. Meaning that for large data dimension, even with the optimal coresets, the KL-divergence is far from optima (zero), implying that the true posterior is not approximated correctly. However, recently few methods have tried to overcome the scalability issue by using lightweight coresets [Bachem et al., 2018].

The Bayesian Pseudo-Coreset (BPC) [Manousakas et al., 2020] approach, as a distinct category of methods, has been proposed to *synthesise* a smaller dataset from the original one, as opposed to selecting a subset, which is the case with coreset methods. The fundamental idea of BPC involves solving an optimization problem over the data space, leading to creation of a 'pseudo' dataset that appropriately approximates the true posterior. The said optimization problem pertains to minimization of a divergence metric between the true posterior and pseudo-coreset posterior. Such a framework removes the constraint for the pseudo-coresets to be a subset of the original dataset. This additional degree of freedom aids in better optimization of the divergence measure. Further, in addition to better approximation of true posterior, pseudo-coreset also come with privacy benefits. Specifically, since pseudo-coresets are not part of original dataset, one can outsource these pseudo-coreset without revealing the original dataset for an user to run inference. Manousakas et al. [2020] also provided theoretical guarantees showing pseudo-coresets are differentially private.

Recently, Kim et al. [2022a] analyzed the BPC construction under different divergence measures such as reverse-KL and Wasserstein divergence. Their analysis revealed that BPC methods under different divergence measures are equivalent to their non-bayesian counterparts. These non-bayesian frameworks are often referred to as 'Dataset Condensation' or 'Dataset Distillation' [Zhao et al., 2021, Zhao and Bilen, 2023, Cazenavette et al., 2022, Wang et al., 2022, Nguyen et al., 2021]. In particular, Kim et al. [2022a] showed that minimization of reverse-KL is equivalent to gradient matching [Zhao et al., 2021] and minimization of wasserstein measure is equivalent to matching training trajectory [Cazenavette et al., 2022]. They also proposed to use forward-KL for better pseudo-coreset construction due to its ability to capture the support of the distribution, contrasting with reverse-KL, which tends to focus on the distribution's modes. However, computing the gradient of forward-KL requires sampling from the intractable pseudo-coreset posterior. While this can be achieved using MCMC methods, the extensive mixing time of MCMC in high-dimensional parameter spaces renders this approach impractical. As a remedy, Gaussian variational approximation around SGD solutions was employed to simplify and expedite the sampling process. However, the quality of such approximation is unknown and remains a matter of concern. Here, we note that the definition of contrastive divergence as presented in Kim et al. [2022a] does not align with the original definition in Hinton [2002]. Specifically, while Kim et al. [2022a] uses forward-KL divergence to arrive at an objective referred to as the contrastive divergence (Section 3.3 of Kim et al. [2022a]), the original definition (in Hinton [2002]) involves difference between two forward-KL divergences. In this work, we resort to the original definition of contrastive divergence as noted in Hinton [2002].

In our current work, we propose a novel approach: using contrastive divergence instead of forward-KL divergence for pseudo-coreset learning. This has two advantages: (1) It eliminates the need for approximating the pseudo-coreset posterior, enabling the straightforward use of MCMC methods, (2) The Markov chain used in this approach does not require extensive mixing to reach a stationary distribution; only a finite number of steps is needed. These advantages effectively address the challenges associated with using forward-KL divergence. Furthermore, our rigorous experiments demonstrate that our proposed method significantly outperforms previous state-of-the-art BPC methods, thereby confirming that the pseudo-coreset posterior using contrastive divergence better approximates the true posterior. Our contributions can be summarized as follows:

- We propose a new framework for the construction of Bayesian Pseudo-Coreset using contrastive divergence.
- The proposed method avoids any approximation of pseudo-coreset posterior and facilitates the use of finite step MCMC methods during learning phase.
- Extensive experimentation reveals that our method surpasses state-of-the-art BPC methods by substantial margins, affirming the better approximation of the true posterior using contrastive divergence.

2 RELATED WORK

2.1 BAYESIAN INFERENCE AND OPTIMIZATION

The objective of Bayesian methods is the model the parameter posterior distribution of a probabilistic model. However, apart from some simple models, the exact posterior distributions are generally intractable [Campbell and Broderick, 2019]. In such scenarios, one often relies on inference techniques like MCMC methods [Robert et al., 1999, Robert and Casella, 2011] and Variational Inference (VI) [Jordan et al., 1998, Wainwright et al., 2008]. Historically, these inference techniques require model-specific tuning based on the path-length parameters, step size [Neal et al., 2011a], and the choice of the variational families [Jaakkola and Jordan, 1997, Jordan et al., 1999]. Recent methods [Ranganath et al., 2014, Kucukelbir et al., 2017, Hoffman et al., 2014] have circumvented these issues by introducing a black box approach that requires only basic specifications about the model. For instance, the traditional variational inference methods [Jaakkola and Jordan, 1997, Jordan et al., 1999] relied on closed form gradients of the model [Ranganath et al., 2014] and an approximate distribution for the posterior of the data. Ranganath et al. [2014], Baydin et al. [2018], Kucukelbir et al. [2017] addressed these issues by employing standard transformation over a multivariate Gaussian distribution and used automatic differentiation techniques to calculate the associated gradients. Similarly, for MCMC methods like Hamiltonian Monte Carlo (HMC) [Neal et al., 2011a] traditional practices involved manually tuning of parameters like step size and path length to achieve accurate posterior estimation. Hoffman et al. [2014] addressed this challenge by automatically estimating both of these parameters.

In many modern applications, these methods are required to scale with the size of the datasets. The standard MCMC algorithms are computationally expensive for large datasets, and the sampling process scales linearly with the data size. Recent works [Bardenet et al., 2017, Korattikara et al., 2014, Maclaurin and Adams, 2014, Welling and Teh, 2011, Ahn et al., 2012, Bierkens et al., 2019, Pollock et al., 2020], have tried to mitigate the computational cost associated with inference models by considering only a random subset of data points during MCMC iterations. One of the initial studies in this direction has been conducted by Welling and Teh [2011] where the authors proposed to use stochastic gradient langevin dynamics (SGLD). This iterative learning algorithm utilizes mini-batches of dataset for Bayesian inference. However, unlike other MCMC methods, their approach often leads to a slow mixing rate. Ahn et al. [2012] addressed this issue by sampling from the Gaussian approximation of posterior for a high mixing rate and mimicking the behavior of SGLD using a pre-conditioner matrix for a slow mixing rate. However, Korattikara et al. [2014], Bardenet et al. [2014] have shown that such a sampling approach often leads to a stationary distribution that can have bounded errors under strong conditions of rapid mixing [Maclaurin and Adams, 2014]. In contrast, they proposed a new accept/reject strategy to select a subset of the dataset for Bayesian inference. On a similar line, Maclaurin and Adams [2014] proposed to use a collection of Bernoulli latent variables to select a subset of the dataset for likelihood estimation. Bierkens et al. [2019], Pollock et al. [2020] have further proposed to use a zig-zag process and quasi-stationary distribution along with the subsampling approaches for bayesian inference.

2.2 BAYESIAN CORESETS

Bayesian coresets [Huggins et al., 2016, Campbell and Broderick, 2018, Campbell and Beronov, 2019, Campbell and Broderick, 2019, Zhang et al., 2021, Naik et al., 2022, Chen et al., 2022] present an alternative strategy to address aforementioned challenges by selecting a small weighted subset of the original dataset which can closely approximate the posterior of the full dataset [Zhang et al., 2021, Huggins et al., 2016]. The idea was introduced in Huggins et al. [2016], where a weighted subset of original data was selected to approximate the log-likelihood of the entire dataset up to some multiplicative error over the parameter space. However, the subset produced by such a technique underestimates the posterior distribution and can result in large approximation errors for some models regardless of the coreset size. Campbell and Broderick [2018] addressed this issue using greedy iterative geodesic ascent (GIGA), that optimally scales the log-likelihood of the coreset to better approximate the entire log-likelihood of the dataset. It further provided a uniform bounded error for all the models. To further enhance the scalability, Campbell and Broderick [2019] tackled the model and data-specific assumptions made in prior work regarding coreset construction. They constructed Bayesian coreset by solving a sparse vector sum based approximation using frank-wolfe [Frank et al., 1956] based solvers. Recent works [Zhang et al., 2021, Naik et al., 2022, Chen et al., 2022] have focused on improving the speed of coreset construction using accelerated optimization methods, quasi-newton refinement, and sparse-hamiltonian flows. However, since the KL divergence between the posteriors of the optimal coreset and the original dataset increases with the data dimensionality [Manousakas et al., 2020], these methods do not easily scale up in high-dimensions.

2.3 BAYESIAN PSEUDO-CORESET

Manousakas et al. [2020] proposed to use a collection of synthetic data to scale the Bayesian inference to high dimensional datasets. Particularly, they frame the problem as divergence minimization between the posteriors associated with the synthetic and the original dataset. The synthetic set generated through this technique is called ‘Bayesian Pseudo-Coreset’ (BPC). Compared to Bayesian coresets, these methods scale more efficiently with data dimensions and yield a more accurate posterior approximation.

Manousakas et al. [2020] formalized the given problem by minimizing the reverse-KL divergence between the posterior of original data and the posterior of synthetic data. On similar lines, Kim et al. [2022a] demonstrated that other divergence metrics, such as Wasserstein distance and forward-KL divergence, can be used to generate pseudo-coreset. In contrast to reverse-KL, which primarily focuses on the modes of the distributions, forward-KL provides a mechanism to better capture the support of the posterior distribution. To efficiently calculate the forward-KL divergence Kim et al. [2022a] used a Gaussian variational approximation of the posterior distribution. However, the quality of such an approximation and its impact on the overall performance of the pseudo-coreset is unknown. Further, computing the gradient of forward-KL requires sampling from an intractable posterior of pseudo-coreset using MCMC methods, which is not straightforward in practice.

2.4 CORESETS AND DATASET CONDENSATION

While Bayesian coreset focuses on selecting data points to facilitate Bayesian inference, coreset selection strategies have been proposed for other algorithms like geometric approximation [Agarwal et al., 2005], mixture models [Feldman et al., 2011], K-means clustering [Feldman and Langberg, 2011, Feldman et al., 2020, Bachem et al., 2016] and DP means [Bachem et al., 2015]. Similarly, for deep learning models, Mirzasoleiman et al. [2020], Killamsetty et al. [2021a,b] have introduced subset selection techniques that leverage gradient matching and meta-learning algorithms. Recent works [Welling, 2009, Castro et al., 2018, Rebuffi et al., 2017, Belouadah and Popescu, 2020, Sener and Savarese, 2017, Farahani and Hekmatfar, 2009], have further proposed strategies to choose a representative and diverse set of samples from the original dataset. These methods aim to create a generic subset by removing redundant data points. Herding-based coreset methods [Welling, 2009, Castro et al., 2018, Rebuffi et al., 2017, Belouadah and Popescu, 2020] select such samples by minimizing the distance between the feature centroids of the coreset, and the original dataset. While K-center-based coreset techniques [Sener and Savarese, 2017, Farahani and Hekmatfar, 2009, Guo et al., 2022] pick the most diverse and representative samples by optimizing a submodular function [Farahani and Hekmatfar, 2009]. Contrary to K-center and herding-based coreset selection methods, forgetting-based coreset [Toneva et al., 2018] removes the easily forgettable samples from the training dataset.

Rather than selecting a subset of data points from the training set, dataset condensation methods aim to generate a synthetic set that emulates the characteristics of the original dataset. For example, in gradient based dataset condensation techniques [Zhao et al., 2021, Yu et al., 2023, Lee et al., 2022, Jiang et al., 2022] the synthetic samples are generated by aligning the gradients of a model trained using original and synthetic datasets. Similarly, meta-learning based methods [Wang et al., 2018, Deng and Russakovsky, 2022, Nguyen et al., 2021, Loo et al., 2022, Zhou et al., 2022] generate these synthetic samples by matching the validation performance of a model trained using the entire dataset with the performance of a model trained using the synthetic set. Cazenavette et al. [2022], Li et al. [2022], Du et al. [2023] propose generating the synthetic dataset using long-horizon trajectories, ensuring that the models learn similar trajectories during optimization. While distribution matching methods [Zhao and Bilen, 2023, Wang et al., 2022, Zhao and Bilen, 2022, Zhao et al., 2023] generate a condensed synthetic set with a similar feature distribution as the original dataset. Recent works [Liu et al., 2023, Zhang et al., 2023, Cazenavette et al., 2023] have further focused on improving the performance and computational complexity of existing dataset condensation techniques by using representative samples from the training set, model augmentation techniques, and generative model for learning the synthetic set. While dataset condensation and BPC might seem to do the same, they are fundamentally different from each other. One can look at Bayesian Pseudo-Coresets as bayesian counterparts of dataset condensation methods. We provide detailed account of differences between dataset condensation methods and BPC methods in Appendix.

3 PROPOSED METHODOLOGY

3.1 BAYESIAN PSEUDO-CORESETS

Consider a dataset $(\mathbf{x}, \mathbf{y}) = \{(\mathbf{x}_i, y_i)\}_{i=1}^{n}$ consisting of n data points. Now consider a synthetic (learnable) dataset $(\tilde{\mathbf{x}}, \tilde{\mathbf{y}}) = \{\tilde{\mathbf{x}}_i, \tilde{y}_i\}_{i=1}^{m}$ such that $\mathbf{y}$ and $\tilde{\mathbf{y}}$ share the same label space and $m \ll n$. Let, $\theta \in \Theta$ be the parameter of a discriminative / classification model. Then the parameter posteriors corresponding to original and synthetic data, $\pi(\theta|\mathbf{x})$ and $\pi(\theta|\tilde{\mathbf{x}})$ are given by

$$\pi_{\mathbf{x}} \triangleq \pi(\theta|\mathbf{x}) = \frac{\pi_0(\theta)}{Z(\mathbf{x})} \exp\left(\sum_{i=1}^{n} \log \pi(y_i|\mathbf{x}_i, \theta)\right) \quad (1)$$

$$\pi_{\tilde{\mathbf{x}}} \triangleq \pi(\theta|\tilde{\mathbf{x}}) = \frac{\pi_0(\theta)}{Z(\tilde{\mathbf{x}})} \exp\left(\sum_{i=1}^{m} \log \pi(\tilde{y}_i|\tilde{\mathbf{x}}_i, \theta)\right) \quad (2)$$

$$= \frac{\pi_0(\theta)}{Z(\tilde{\mathbf{x}})} \exp\left(-E(\tilde{\mathbf{x}}, \theta)\right) \quad (3)$$

where,

$$Z(\mathbf{x}) = \int_{\Theta} \pi_0(\theta) \exp\left(\sum_{i=1}^{n} \log \pi(y_i|\mathbf{x}_i, \theta)\right) d\theta \quad (4)$$

$$Z(\tilde{\mathbf{x}}) = \int_{\Theta} \pi_0(\theta) \exp\left(-E(\tilde{\mathbf{x}}, \theta)\right) d\theta \quad (5)$$

are appropriate normalizing constants. Here, $\pi_0(\theta)$ is the prior distribution and $E(\tilde{\mathbf{x}}, \theta) = -\sum_{i=1}^{m} \log \pi(\tilde{y}_i|\tilde{\mathbf{x}}_i, \theta)$ is the sum of negative log-likelihoods which can be treated as a generic potential or energy function. Since n is often very large, the posterior estimation using $\pi_{\mathbf{x}}$ is computationally expensive and infeasible. However, an appropriate approximation such as $\pi_{\tilde{\mathbf{x}}}$ where $m \ll n$, allows one to overcome this hurdle. In particular, this approximation is carried out by solving the following optimization problem:

$$\tilde{\mathbf{x}}^* = \arg\min_{\tilde{\mathbf{x}}} \; D\left(\pi_{\mathbf{x}}, \pi_{\tilde{\mathbf{x}}}\right) \tag{6}$$

where, $D(\cdot,\cdot)$ is a divergence measure between two distributions. Recently, Kim et al. [2022a] showed the results for above optimization problem under different divergence metrics. Specifically, they analyzed the results with reverse-KL and wasserstein divergence; consequently drawing equivalence with dataset condensation methods like gradient matching [Zhao et al., 2021] and MTT [Cazenavette et al., 2022]. Further, they propose an alternative solution by using forward-KL divergence as it encourages a model to cover the entire target distribution in contrast to reverse-KL which encourages mode capturing models. The gradient of the forward-KL divergence, as derived in Kim et al. [2022a], is expressed as follows:

$$\nabla_{\tilde{\mathbf{x}}} D_{KL}\left(\pi_{\mathbf{x}} || \pi_{\tilde{\mathbf{x}}}\right) = \mathbb{E}_{\pi_{\tilde{\mathbf{x}}}}\left[-\nabla_{\tilde{\mathbf{x}}} E(\tilde{\mathbf{x}}, \theta)\right] + \nabla_{\tilde{\mathbf{x}}} \mathbb{E}_{\pi_{\mathbf{x}}}\left[E(\tilde{\mathbf{x}}, \theta)\right] \tag{7}$$

This gradient computation necessitates the calculation of expectations with respect to the probability distributions $\pi_{\mathbf{x}}$ and $\pi_{\tilde{\mathbf{x}}}$. However, the presence of intractable partition functions ($Z(\mathbf{x})$ and $Z(\tilde{\mathbf{x}})$) poses challenges in efficiently sampling from these posterior distributions. One can resort to MCMC methods such as langevin dynamics or hamiltonian monte-carlo for sampling, however, due to large dimension of Θ-space, the mixing-time of these methods is very large and in-efficient in practice. To overcome this issue, Kim et al. [2022a] employs gaussian variational approximations for these posteriors, rendering the sampling process computationally feasible. Specifically, gaussian distributions are used, centered around parameters obtained from Stochastic Gradient Descent (SGD) trajectories of $\mathbf{x}$ and $\tilde{\mathbf{x}}$ (cf. [Kim et al., 2022a] for details).

In practice, since m (number of samples in pseudo-coreset) is generally very small, the SGD trajectories of $\tilde{\mathbf{x}}$ might overfit, leading to erroneous approximations. Hence, it can be seen that there is a clear trade-off between 'posterior approximation quality' and 'computational efficiency' in the previous methods (cf. Table 7 for quantitative numbers). Therefore, it is preferable to bypass such approximations and sample directly from the exact posteriors. In this work, we propose to work with contrastive divergence [Hinton, 2002] instead of forward-KL to construct the pseudo-coreset. Specifically, using contrastive divergence leads to a loss objective where $\pi_{\tilde{\mathbf{x}}}$ can be used as it is without any approximation. The key idea behind this is that instead of minimizing forward-KL, contrastive divergence minimizes difference between two forward-KL terms, that results in cancellation of expectation w.r.t $\pi_{\tilde{\mathbf{x}}}$ allowing us to circumvent this approximation. We describe this in detail in next section.

3.2 CONTRASTIVE DIVERGENCE FOR BPC

As mentioned earlier, we propose to work with contrastive divergence instead of forward-KL for construction of pseudo-coresets. The concept of contrastive divergence was initially introduced by seminal work in Hinton [2002].The central premise behind contrastive divergence hinges on a straightforward insight: whereas minimizing forward KL divergence necessitates a term that involves sampling from $\pi_{\tilde{\mathbf{x}}}$, minimizing the difference between two forward KL divergences leads to the nullification of this term. More explicitly, the contrastive divergence is defined as:

$$\mathcal{L}_{CD} = D_{KL}(\pi_{\mathbf{x}} || \pi_{\tilde{\mathbf{x}}}) - D_{KL}(\Pi_E^k \pi_{\mathbf{x}} || \pi_{\tilde{\mathbf{x}}}) \tag{8}$$

where, $\Pi_E^k(\cdot)$ is an MCMC transition kernel for $\pi_{\tilde{\mathbf{x}}}$ and $\Pi_E^k \pi_{\mathbf{x}}$ represents k sequential MCMC transitions starting from $\pi_{\mathbf{x}}$. Here, we use transition kernel in the context of Markov process. Particularly, a one-step transition kernel is a map that takes a state as input and generates the next state after one step. Similarly, a k-step transition kernel takes a state as input and generates the state after k-steps. This is akin to the role of transition matrix in markov chains with finite states. In context of the proposed method, the k-step transition kernel takes a state sampled from $\pi_{\mathbf{x}}$, and generates a state after k-steps. Additionally, we note that Eq. 8 is minimized to zero only if $\pi_{\mathbf{x}} = \pi_{\tilde{\mathbf{x}}}$. This is a well known result noted in Hinton [2002] (cf Page 4 of Hinton [2002]).

For brevity, let us denote $\bar{\pi}_{\mathbf{x}}$ as $\Pi_E^k \pi_{\mathbf{x}}$. As shown in Hinton [2002], the gradient of the above objective is approximately given by [1]:

$$\nabla_{\tilde{\mathbf{x}}} \mathcal{L}_{CD} = \mathbb{E}_{\pi_{\mathbf{x}}}\left[\nabla_{\tilde{\mathbf{x}}} E(\tilde{\mathbf{x}}, \theta)\right] - \mathbb{E}_{\bar{\pi}_{\mathbf{x}}}\left[\nabla_{\tilde{\mathbf{x}}} E(\tilde{\mathbf{x}}, \theta)\right] \tag{9}$$

It is worth noting that the gradient estimation in the above equation does not necessitate sampling from $\pi_{\tilde{\mathbf{x}}}$. Instead, it calls for sampling from $\pi_{\mathbf{x}}$ and $\bar{\pi}_{\mathbf{x}}$. In this context, we can employ a variational posterior to approximate $\pi_{\mathbf{x}}$ and use MCMC sampling techniques (e.g. langevin dynamics [Bohdal et al., 2020]) starting from $\pi_{\mathbf{x}}$ to sample from $\bar{\pi}_{\mathbf{x}}$. Notably, unlike in Eq. 7, the MCMC sampling utilized here only needs to run for finite k steps, alleviating the requirement for substantial Markov chain mixing.

In particular, we use gaussian variational posterior ($q_{\mathbf{x}}$) to approximate $\pi_{\mathbf{x}}$. Then, a k-step MCMC starting from $q_{\mathbf{x}}$

[1]Please note that the signs in this expression are opposite to those presented in Kim et al. [2022a], primarily due to differences in the treatment of the energy function. In Kim et al. [2022a], the energy function (referenced as Eq. 2 in their paper) is considered positive, whereas in our work, we adopt a convention where the energy function (as represented in Eq. 3 of our paper) is negative. This choice is made for convenience, aligning with the convention in physics literature where lower energy states are typically considered stable.

should be used as a variational substitute for $\bar{\pi}_{\mathbf{x}}$:

$$q_{\mathbf{x}}(\theta) = \mathcal{N}(\theta; \theta_{\mathbf{x}}, \Sigma_{\mathbf{x}}), \quad \bar{q}_{\mathbf{x}}(\theta) = \Pi_E^k \, q_{\mathbf{x}}(\theta) \tag{10}$$

where, $\theta_{\mathbf{x}}$ is the MAP solution computed for $\mathbf{x}$. Here, one can note that making an approximation for $\pi_{\mathbf{x}}$ is enough unlike previous methods where additional approximations for $\pi_{\tilde{\mathbf{x}}}$ is also required. Hence, the final gradient estimate is obtained as

$$\nabla_{\tilde{\mathbf{x}}}\mathcal{L}_{CD} \approx \mathbb{E}_{q_{\mathbf{x}}}\left[\nabla_{\tilde{\mathbf{x}}}E(\tilde{\mathbf{x}}, \theta)\right] - \mathbb{E}_{\bar{q}_{\mathbf{x}}}\left[\nabla_{\tilde{\mathbf{x}}}E(\tilde{\mathbf{x}}, \theta)\right] \tag{11}$$

$$\approx \nabla_{\tilde{\mathbf{x}}} \frac{1}{N} \sum_{j=1}^{N} \left[E\left(\tilde{\mathbf{x}}, \theta_{\mathbf{x}} + \Sigma_{\mathbf{x}}^{1/2} \varepsilon_{\mathbf{x}}^{(j)}\right) - E\left(\tilde{\mathbf{x}}, \mathrm{sg}\left(\bar{\theta}^{(j)}\right)\right)\right] \tag{12}$$

where, $\mathrm{sg}(\cdot)$ denotes stop-gradient operator, $\varepsilon_{\mathbf{x}}^{(j)} \sim \mathcal{N}(0, I)$ and $\bar{\theta}^{(j)}$ is obtained via running k-step MCMC starting from $\left(\theta_{\mathbf{x}} + \Sigma_{\mathbf{x}}^{1/2}\varepsilon_{\mathbf{x}}^{(j)}\right)$.

Here, we note that one can theoretically learn $\Sigma_{\mathbf{x}}$ by treating it as a learnable parameter. However, this would require gradient of determinant of the covariance matrix. Given the high dimensional parameter space, this operation would lead to computational inefficiencies. Hence, we treat it as a hyperparameter and keep it fixed.

Further, for computational efficiency, we assess the parameter posterior with $\mathbf{x}$ using expert trajectories similar to Kim et al. [2022a]. In essence, expert trajectories represent sequences of parameters obtained while training a model on the dataset $(\mathbf{x}, \mathbf{y})$. Each of these sequences is termed as 'parameter trajectory,' and the collection of these trajectories, acquired through various training instances, is known as 'expert trajectories.' This eliminates the need to compute MAP solutions for $\mathbf{x}$ ($\theta_{\mathbf{x}}$) at each training step. During training, we randomly pick a parameter from these trajectories to calculate the objective function.

4 EXPERIMENTS AND RESULTS

4.1 EVALUATION DETAILS

We evaluate our method both quantitatively and qualitatively on several BPC-benchmark datasets with different compression ratios, i.e., the number of images generated per class (ipc). In particular, we perform our experiments on six different datasets, namely, CIFAR10 [Krizhevsky and Hinton, 2009], SVHN [Sermanet et al., 2012], MNIST [LeCun et al., 1998], FashionMNIST [Xiao et al., 2017], CIFAR100 [Krizhevsky and Hinton, 2009] and Tiny Imagenet (T-Imagenet) [Le and Yang, 2015]. All the experiments perform multi-class classification tasks with ipc=1, 10, and 50 which is in line with previous baselines.We employ Langevin dynamics [Neal et al., 2011b, Teh et al., 2003] during training as well as inference and report accuracy (Acc) and negative log-likelihood (NLL) with respect to the ground truth labels. For our primary experiments, we use a CNN architecture (ConvNet) exactly as described in the previous works [Kim et al., 2022b, Manousakas et al., 2020, Cazenavette et al., 2023] (cf. Appendix for details) for a fair comparison.

Further, we assess the robustness of the BPC methods on out-of-distribution dataset and against adversarial attacks in Section 4.4. We also examine the cross-architecture performance of the proposed method in Section 4.5. Next, since bayesian methods are often sensitive to the number of parameters being sampled from the posterior, we observe the effect of number of parameters on the proposed method and compare it with previous BPC baselines in Section 4.6. Further, we provide an ablation study of the proposed method against different hyperparameters in Section 4.7. Lastly, we provide a quantitative comparison of quality of posterior parameter samples in Section 4.8. We refer the reader to Appendix for details regarding these experiments.

4.2 BASELINES AND COMPARISONS

We consider the state-of-the-art BPC methods using reverse-KL (BPC-rKL), forward-KL (BPC-fKL), and Wasserstein distance (BPC-W) [Kim et al., 2022a, Manousakas et al., 2020] for comparison. Further comparison with other coreset methods and dataset condensation is provided in the Appendix. All the baselines are implemented using the official codebase provided by respective methods if available, otherwise, we directly take the reported numbers. In cases, neither the codebase nor the numbers are reported, we exclude them from our tables.

4.3 RESULTS AND COMPARISON

Table 1 presents the results of the comparative analysis between our approach and other BPC baselines. We observe that the proposed method significantly outperforms all the BPC baselines by large margins. For instance, we observe an improvement of 11.3%, 6.54%, and 21.01% in accuracy for CIFAR10 with ipc values of 1, 10, and 50, respectively. Additionally, there is a decrease of 0.1 and 0.01 points in negative log-likelihood for ipc values of 1 and 10, respectively, in comparison to the best-performing BPC baseline. Similarly, on SVHN, we notice an improvement in accuracy and negative log-likelihood. Specifically, we observe gains of 18.72%, 6.83% in accuracy and reduction of 0.06, 0.03 point in negative log-likelihood for ipc 1, 10 respectively, compared to the BPC counterparts. A similar trend can be seen for MNIST and FMNIST as well [2]. We attribute

[2]We observe that the proposed method has smaller variance compared to other methods. Upon analysis, we attribute this behavior to the rapid decrease in the gradient of the energy function $((\nabla_\theta E(\theta, \tilde{\mathbf{x}}))$ with respect to parameters in langevin dynamics.

Table 1: Comparison of the proposed method with BPC baselines. The results are noted in the form of (mean $\pm$ std. dev) where we have obtained test accuracy over five independent runs on the pseudo-coreset. The best performer across all methods is denoted in bold ($\boldsymbol{x \pm s}$).

	ipc	Ratio(%)	BPC-rKL(sghmc)		BPC-W (sghmc)		BPC-fKL (hmc)		BPC-fKL (sghmc)		Ours	
			Acc(↑)	NLL(↓)	Acc(↑)	NLL(↓)	Acc(↑)	NLL(↓)	Acc(↑)	NLL(↓)	Acc(↑)	NLL(↓)
MNIST	1	0.017	74.80 ± 1.17	1.90 ± 0.01	83.59 ± 1.49	1.91 ± 0.02	90.46 ± 1.50	1.54 ± 0.03	82.98 ± 2.20	1.87 ± 0.03	$\mathbf{93.42 \pm 0.09}$	$\mathbf{1.53 \pm 0.01}$
	10	0.17	95.27 ± 0.17	1.53 ± 0.01	91.72 ± 0.55	1.52 ± 0.01	89.80 ± 0.82	1.52 ± 0.01	92.05 ± 0.42	$\mathbf{1.51 \pm 0.02}$	$\mathbf{97.71 \pm 0.24}$	1.57 ± 0.02
	50	0.83	94.18 ± 0.26	1.36 ± 0.02	93.72 ± 0.55	1.48 ± 0.02	95.58 ± 1.63	1.37 ± 0.02	93.63 ± 1.80	1.36 ± 0.02	$\mathbf{98.91 \pm 0.22}$	$\mathbf{1.36 \pm 0.01}$
FMNIST	1	0.017	70.53 ± 1.09	2.47 ± 0.02	72.39 ± 0.87	2.10 ± 0.01	$\mathbf{78.24 \pm 1.02}$	1.95 ± 0.04	72.51 ± 2.53	2.30 ± 0.02	77.29 ± 0.50	$\mathbf{1.90 \pm 0.03}$
	10	0.17	78.81 ± 0.17	1.64 ± 0.01	83.69 ± 0.51	1.64 ± 0.03	82.06 ± 0.44	$\mathbf{1.53 \pm 0.02}$	83.29 ± 0.55	1.54 ± 0.03	$\mathbf{88.40 \pm 0.21}$	1.56 ± 0.01
	50	0.83	76.97 ± 0.59	1.48 ± 0.02	74.41 ± 0.48	1.52 ± 0.03	82.40 ± 0.35	1.32 ± 0.02	74.82 ± 0.52	1.47 ± 0.02	$\mathbf{89.47 \pm 0.06}$	$\mathbf{1.30 \pm 0.02}$
SVHN	1	0.014	18.34 ± 1.79	3.01 ± 0.02	33.52 ± 1.15	2.89 ± 0.01	48.02 ± 5.62	2.44 ± 0.03	21.48 ± 6.58	2.57 ± 0.02	$\mathbf{66.74 \pm 0.09}$	$\mathbf{2.38 \pm 0.04}$
	10	0.14	60.68 ± 5.07	2.00 ± 0.01	74.75 ± 1.27	1.95 ± 0.02	65.64 ± 2.92	2.13 ± 0.01	75.49 ± 0.84	1.84 ± 0.01	$\mathbf{82.32 \pm 0.56}$	$\mathbf{1.81 \pm 0.01}$
	50	0.7	78.27 ± 0.62	1.89 ± 0.01	79.49 ± 0.54	1.90 ± 0.01	79.60 ± 0.53	1.86 ± 0.01	77.08 ± 1.80	$\mathbf{1.72 \pm 0.01}$	$\mathbf{88.41 \pm 0.12}$	1.88 ± 0.02
Cifar10	1	0.02	21.62 ± 0.83	2.57 ± 0.01	29.34 ± 1.21	2.14 ± 0.03	35.57 ± 0.95	1.97 ± 0.03	29.30 ± 1.10	2.10 ± 0.03	$\mathbf{46.87 \pm 0.20}$	$\mathbf{1.87 \pm 0.02}$
	10	0.2	37.89 ± 1.54	2.13 ± 0.02	48.90 ± 1.72	1.73 ± 0.02	43.07 ± 1.06	1.89 ± 0.02	49.85 ± 1.37	1.73 ± 0.01	$\mathbf{56.39 \pm 0.70}$	$\mathbf{1.72 \pm 0.03}$
	50	1	37.54 ± 1.32	1.93 ± 0.03	46.17 ± 0.67	1.62 ± 0.02	50.92 ± 1.49	1.70 ± 0.03	42.30 ± 2.87	$\mathbf{1.54 \pm 0.01}$	$\mathbf{71.93 \pm 0.17}$	1.57 ± 0.03
Cifar100	1	0.2	3.56 ± 0.04	4.69 ± 0.02	12.19 ± 0.22	4.20 ± 0.01	7.57 ± 0.54	4.25 ± 0.04	12.07 ± 0.16	4.27 ± 0.02	$\mathbf{23.97 \pm 0.11}$	$\mathbf{4.01 \pm 0.02}$
	10	2	-		-		-		-	-	$\mathbf{28.42 \pm 0.24}$	$\mathbf{3.14 \pm 0.02}$
T-ImageNet	1	0.2	-		-		-		-	-	$\mathbf{8.39 \pm 0.07}$	$\mathbf{4.72 \pm 0.01}$
	10	2	-		-		-		-	-	$\mathbf{17.82 \pm 0.39}$	$\mathbf{3.64 \pm 0.05}$

(a) Images generated with ipc=1 for MNIST

(c) Images generated with ipc=1 for FMNIST

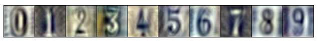
(e) Images generated with ipc=1 for SVHN

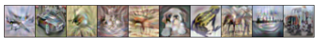
(g) Images generated with ipc=1 for CIFAR10

(b) Images generated with ipc=10 for MNIST

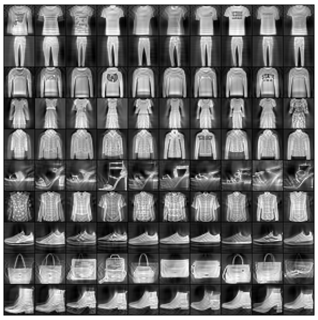
(d) Images generated with ipc=10 for FMNIST

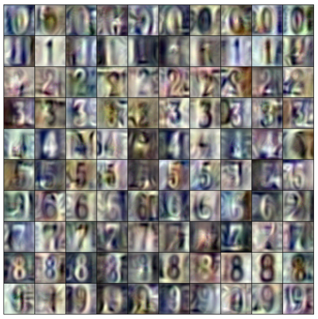
(f) Images generated with ipc=10 for SVHN

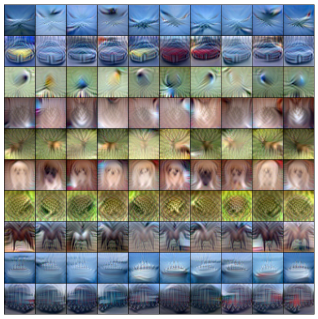
(h) Images generated with ipc=10 for CIFAR10

Figure 1: Visualizations of pseudo-coreset generated from our method with one image per class (top) and ten images per class (bottom) for MNIST, FMNIST, SVHN and CIFAR10. It can be seen that the class labels are identifiable to a large extent.

this boost in performance to the flexible formulation of the proposed method.

We present the qualitative visualizations for MNIST, FMNIST, SVHN, and CIFAR10 datasets with 1 image per class and 10 image per class in Fig. 1. It can be seen that the constructed pseudo-coreset is identifiable but inherits some artifacts due to the constraints on the dataset size. As the number of images per class increases, the model can induce more variations across all the classes and thus produce a diverse pseudo-coreset. Additional qualitative visualizations for pseudo-coreset generated with 50 images per class on CIFAR100 and T-ImageNet dataset are presented in the Appendix.

This indicates that the sampled parameter stays near the initial parameter value from the expert trajectory, which is based on confident predictions derived from SGD trajectories trained on the full dataset. Therefore, the reduced variance observed is likely a result of this confidence.

4.4 RESULTS ON OUT OF DISTRIBUTION (OOD) DATASET

We present the results of the proposed method on out-of-distribution (OOD) dataset in Table 2. We use CIFAR10-C [Hendrycks and Dietterich, 2019] dataset for this experiment. In particular, we sample the parameters from the pseudo-coreset posterior obtained using clean CIFAR10 (ipc=10) and perform inference on the corrupted CIFAR10-C, which consists of CIFAR10 images afflicted with different types of corruption including Gaussian Blur, Gaussian

Noise, etc. It is evident from Table 2 that our method demonstrates robustness to various types of corruption and exhibits superior performance compared to other baselines. Notably, for corruptions like Gaussian Blur, our method achieves a 1.63% increase in accuracy and a 0.17-point reduction in negative log-likelihood compared to the best-performing BPC baseline. Likewise, for JPEG Compression, Zoom Blur, and Defocus Blur, our method yields an improvement of 0.07%, 2.08%, and 0.43% in accuracy, along with a reduction of 0.14, 0.05, and 0.06 points in negative log-likelihood, respectively. The robustness of the proposed method to different forms of corruption highlights its ability to provide a better approximation of underlying posterior distribution when compared to other baselines.

We further test all the BPC methods against ℓ_∞ adversarial attack [Croce et al., 2021]. We report the clean accuracy and robust accuracy respectively for each method. Our observations could be found in Table 3. We see that under ℓ_∞ attack, the performance of all BPC methods drop significantly. This is perhaps due to the fact that these methods don't explicitly take robustness into account while constructing pseudo-coresets. However, we observe even under performance drop, our method gives best robust accuracy as compared to other BPC methods.

4.5 RESULTS ON CROSS-ARCHITECTURE EXPERIMENTS

Here, we present the cross-architecture results pertaining to various BPC methods. In these experiments, we construct the pseudo-coreset using the said ConvNet model, while during inference, we use different architectures such as ResNet [He et al., 2016b], VGG-Net [Simonyan and Zisserman, 2014] and AlexNet [Krizhevsky et al., 2017a] for evaluation. We perform these experiments for CIFAR10 (ipc = 10). The results of the cross-architecture experiments are presented in Table 4. It can be seen that previous BPC methods fail to generalize across different network architectures, whereas our method demonstrates the ability to adapt to various architectures. For instance, the performance of BPC-fKL and BPC-rKL drop by 34.19% and 24.42% respectively on ResNet, resulting in random predictions with an accuracy of almost 10%, whereas our method observes a drop of only 14.74% while giving an accuracy of 41.65%.

4.6 EFFECT OF DIFFERENT NUMBER OF PARAMETERS

Lastly, we analyze the performance of BPC methods across differently parameterized networks. Specifically, we generate pseudo-coresets for CIFAR10 (ipc=10) by employing ConvNets with different parameter configurations. These configurations encompass ConvNets with different depth and width. We also conduct a comparative analysis with other deep learning architectures, including AlexNet [Krizhevsky et al., 2017a], VGG11 [Simonyan and Zisserman, 2014], and ResNet [He et al., 2016b]. Bayesian inference techniques generally encounter scalability issues when dealing with large parametric networks [Jospin et al., 2022]. This experiment is conducted to ascertain the impact of both large and small architectures on the performance of pseudo-coresets.

The results for different parameterized architectures are presented in Table 5. Here, CN-DxWy denotes a ConvNet architecture with a depth of 'x' and width of 'y'. It is evident from the results that the performance of all BPC methods declines as the number of parameters in the architectures increases. However, our model exhibits relatively better performance in comparison to other methods. Specifically, while our method demonstrates a 7.72% decrease in performance for the ResNet architecture, other BPC baselines such as BPC-fKL, BPC-W, and BPC-rKL experience declines of approximately 14.75%, 16.06%, and 12.91%, respectively. This observation underscores the greater tolerance of our method to large parametric models when compared to other baselines. We again highlight that the performance gain achieved by our proposed method can be attributed to the current formulation, which can generate better approximation to the true posterior.

4.7 ABLATION STUDY

Next, we provide an empirical analysis of the effect of different hyperparameters on the proposed method. Particularly, we observe that there are two key hyperparameters that affect the performance of the proposed method: the covariance matrix $\Sigma_{\mathbf{x}}$ (see Eq. 10) and the number of MCMC steps k (see Eq. 8). Hence, we ablate our method against these two important hyperparameters and report the results in Table 6.

Further, we verify our claim that the proposed method provides a good trade-off between performance and computational cost. Particularly, as seen in Eq. 7, one can resort to MCMC methods to evaluate the second term of the said expression, however, since this can be computationally expensive in the high-dimensional parameter space, we resort to using contrastive-divergence that allows one to use finite step MCMC steps making the proposed method computationally less expensive. To verify this, we compare our method against pseudo-coresets obtained using Eq. 7 alongwith MCMC methods. Particularly, we employ HMC [Chen et al., 2014] and Kronecker-Factorised Laplace (KFL) [Ritter et al., 2018] for this purpose. Our observations are noted in Table 7.We compare GPU Memory usage, Iteration time and Accuracy for each of these method against ours. We see that both HMC and KFL consume more memory and time compared to our method. However, HMC provides marginally better result and KFL gives slightly worse result compared to our method. This verifies our claim.

Table 2: Comparison of the proposed method with BPC baselines for the performance on out-of-distribution data. The classifier model is trained on pseudo-coresets generated using CIFAR10. However, the model is evaluated on CIFAR10-C dataset with different types of corruption.

Corruption	BPC-rKL (sghmc)		BPC-W (sghmc)		BPC-fKL (hmc)		BPC-fKL (sghmc)		Ours	
	Acc(↑)	NLL(↓)	Acc(↑)	NLL(↓)	Acc(↑)	NLL(↓)	Acc(↑)	NLL(↓)	Acc(↑)	NLL(↓)
Gaussian Blur	31.02 ± 2.65	2.13 ± 0.77	35.66 ± 1.21	2.04 ± 0.12	34.76 ± 1.86	1.89 ± 0.04	39.73 ± 2.72	1.94 ± 0.05	$\mathbf{41.36 \pm 0.72}$	$\mathbf{1.73 \pm 0.83}$
Gaussian Noise	25.49 ± 1.89	2.28 ± 0.08	33.21 ± 0.89	2.11 ± 0.03	36.70 ± 1.01	1.86 ± 0.02	35.71 ± 2.29	2.00 ± 0.05	$\mathbf{38.01 \pm 1.26}$	$\mathbf{1.82 \pm 0.11}$
JPEG Compression	30.40 ± 0.90	2.13 ± 0.02	26.33 ± 1.34	2.26 ± 0.04	36.20 ± 1.92	1.85 ± 0.03	37.26 ± 2.87	1.95 ± 0.06	$\mathbf{37.33 \pm 0.19}$	$\mathbf{1.71 \pm 0.03}$
Snow	26.85 ± 1.71	2.20 ± 0.07	37.50 ± 3.50	1.93 ± 0.08	33.99 ± 1.91	$\mathbf{1.91 \pm 0.03}$	35.68 ± 2.71	2.00 ± 0.07	$\mathbf{37.84 \pm 0.64}$	1.91 ± 0.05
Impulsive Noise	28.39 ± 1.48	2.15 ± 0.06	36.71 ± 1.93	1.96 ± 0.05	33.81 ± 1.58	1.94 ± 0.02	$\mathbf{38.26 \pm 2.34}$	1.92 ± 0.05	37.98 ± 2.15	$\mathbf{1.89 \pm 0.07}$
Zoom Blur	31.74 ± 1.24	2.09 ± 0.04	36.22 ± 2.08	1.99 ± 0.05	31.30 ± 3.64	1.98 ± 0.08	35.05 ± 2.90	2.04 ± 0.07	$\mathbf{38.30 \pm 0.77}$	$\mathbf{1.93 \pm 0.13}$
Pixelate	28.98 ± 2.26	2.19 ± 0.07	27.98 ± 1.77	2.20 ± 0.05	35.59 ± 1.94	$\mathbf{1.88 \pm 0.03}$	$\mathbf{39.14 \pm 3.15}$	1.93 ± 0.06	38.97 ± 1.51	1.92 ± 0.07
Speckle Noise	29.88 ± 0.59	2.09 ± 0.02	33.33 ± 2.18	2.05 ± 0.05	34.37 ± 2.02	1.90 ± 3.57	40.54 ± 1.93	$\mathbf{1.89 \pm 0.04}$	$\mathbf{42.66 \pm 0.83}$	1.95 ± 0.03
Defocus Blur	27.57 ± 1.31	2.20 ± 0.05	33.80 ± 4.21	2.09 ± 0.11	33.60 ± 2.93	1.93 ± 0.06	36.72 ± 3.68	1.99 ± 0.08	$\mathbf{37.15 \pm 1.03}$	$\mathbf{1.87 \pm 0.04}$
Motion Blur	17.38 ± 2.51	2.73 ± 0.14	35.22 ± 3.35	2.01 ± 0.08	34.33 ± 1.89	1.92 ± 0.04	35.24 ± 3.30	2.01 ± 0.05	$\mathbf{37.06 \pm 0.49}$	$\mathbf{1.92 \pm 0.04}$

Table 3: Comparison of the proposed method with BPC baselines for the performance against ℓ_∞ attack on CIFAR10 with 10 ipc.

BPC-rkl		BPC-W		BPC-fkl		Ours	
Clean Acc	Robust Acc	Clean Acc	Robust Acc	Clean Acc	Robust Acc	Clean Acc	Robust Acc
37.89 ± 1.54	13.54 ± 1.21	48.90 ± 1.72	15.62 ± 0.92	49.85 ± 1.37	19.30 ± 1.39	$\mathbf{56.39 \pm 0.70}$	$\mathbf{22.81 \pm 1.28}$

Table 4: Cross-architecture generalization analysis of BPC methods.

	ConvNet	ResNet	VGG	AlexNet
Ours	$\mathbf{56.39 \pm 0.70}$	$\mathbf{41.65 \pm 1.03}$	$\mathbf{47.51 \pm 0.89}$	$\mathbf{30.58 \pm 1.43}$
BPC-fKL(hmc)	44.34 ± 1.11	10.15 ± 0.21	10.43 ± 0.33	12.21 ± 0.18
BPC-rKL(sghmc)	34.48 ± 0.48	10.06 ± 0.08	10.26 ± 0.35	11.02 ± 0.12

Table 5: Performance comparison of the proposed method and other BPC baselines for different parameterized architectures.

Methods	CN-D3W128	CN-D3W256	CN-D5W128	AlexNet	VGG11	ResNet
	320,010	1,229,834	596,490	1,872,202	9,231,114	11,173,962
Ours	$\mathbf{56.39 \pm 0.70}$	$\mathbf{55.93 \pm 1.30}$	$\mathbf{56.01 \pm 0.69}$	$\mathbf{52.88 \pm 1.39}$	$\mathbf{49.26 \pm 2.33}$	$\mathbf{48.67 \pm 0.52}$
BPC-rKL (sghmc)	37.89 ± 1.54	35.82 ± 1.88	35.92 ± 1.88	32.60 ± 1.45	27.66 ± 0.73	24.98 ± 1.53
BPC-W (sghmc)	48.90 ± 1.72	43.71 ± 1.42	46.01 ± 0.92	39.01 ± 0.51	35.11 ± 1.82	32.84 ± 1.38
BPC-fKL (hmc)	49.85 ± 1.37	45.87 ± 0.78	47.92 ± 1.27	41.22 ± 1.62	37.05 ± 1.24	35.10 ± 2.03

Table 6: Ablation study of the proposed method against different hyperparameters on CIFAR10 with 10 ipc.

Ablation on $\Sigma_{\mathbf{x}}$					
$\Sigma_{\mathbf{x}}^{1/2} = 0.01I$		$\Sigma_{\mathbf{x}}^{1/2} = 0.001I$		$\Sigma_{\mathbf{x}}^{1/2} = 0.0001I$	
Acc	NLL	Acc	NLL	Acc	NLL
50.18 ± 0.50	1.94 ± 0.05	$\mathbf{56.39 \pm 0.70}$	$\mathbf{1.72 \pm 0.03}$	54.18 ± 0.23	1.86 ± 0.02

Ablation on k (or L in Algorithm 1)					
$k = 10$		$k = 50$		$k = 100$	
Acc	NLL	Acc	NLL	Acc	NLL
43.77 ± 0.98	1.78 ± 0.02	51.27 ± 1.01	1.78 ± 0.02	$\mathbf{56.39 \pm 0.70}$	$\mathbf{1.72 \pm 0.03}$

Table 7: Efficiency and Accuracy comparison of the proposed method against pseudo-coresets obtained via direct MCMC estimation of second term of Eq. 7 on CIFAR10 with 10 ipc.

HMC [Chen et al., 2014]			**KFL** [Ritter et al., 2018]			**Ours**		
GPU (GB)	Time (s)	Acc	GPU (GB)	Time (s)	Acc	GPU (GB)	Time (s)	Acc
52.67	13.82	57.09	61.05	20.17	53.98	38.28	0.75	56.39

4.8 COMPARISON OF POSTERIOR QUALITY

Lastly, we provide a quantitative comparison for the quality of posteriors obtained using our method and other baselines to substantiate our claims. Note that the true parameter posteriors are intractable and are generally unknown for complex deep networks. Hence, it is difficult to make comparisons against such gold standard posterior for complex networks.

Table 8: Comparison of ECE (↓) and Brier Score (↓) for the proposed method against other baselines

BPC-rkl		BPC-W		BPC-fkl		Ours	
ECE	Brier Score	ECE	Brier Score	ECE	Brier Score	ECE	Brier Score
0.1183 ± 0.0038	0.7988 ± 0.0038	0.1457 ± 0.0110	0.8030 ± 0.0049	0.1538 ± 0.0049	0.7231 ± 0.0049	$\mathbf{0.1092 \pm 0.0052}$	$\mathbf{0.6755 \pm 0.0042}$

However, to provide a comprehensive understanding of the quality of our obtained posteriors, we report the Expected Calibration Error (ECE) [Naeini et al., 2015] and Brier score [Brier, 1950]. These metrics, akin to those presented in Table 6 of Kim et al. [2022a], serve as well-established benchmarks for evaluating posterior quality. These results are listed in Table 8. We see that the proposed method performs the best amongst all the baselines, further ensuring that the proposed method is effective in the qualitative sense as well.

5 CONCLUSION

In this work, we propose a novel approach to generate pseudo-coreset using contrastive divergence. Our approach addresses the need to approximate the posterior of pseudo-coreset and uses a finite number of steps in MCMC methods to sample the parameters from the underlying posterior distribution. Subsequently, these parameters are used to construct pseudo-coreset via contrastive divergence. The empirical evidence presented in our study illustrates that our proposed method surpasses previous BPC baselines by substantial margins across multiple datasets.

***Limitations and Future Work*:** While our approach effectively removes variational assumptions associated with the pseudo-coreset posterior and utilizes MCMC methods for parameter sampling, our study still relies on certain assumptions about the posterior of the original dataset. Since there remains a significant performance gap between the pseudo-coreset and the original dataset, a potential avenue for future research could be to relax these assumptions to enhance the performance of BPC methods.

***Broader Impact*:** BPC methods have positive applications in democratization and privacy-related concerns by reducing the dependence on the original dataset. We don't believe that our method has any associated negative societal impact.

Acknowledgements

This work was supported (in part for setting up the GPU compute) by the Indian Institute of Science through a start-up grant. Prathosh is supported by Infosys Foundation Young investigator award. Piyush is supported by Government of India via Prime minister's research fellowship.

References

Pankaj K Agarwal, Sariel Har-Peled, Kasturi R Varadarajan, et al. Geometric approximation via coresets. *Combinatorial and computational geometry*, 52(1):1–30, 2005.

Sungjin Ahn, Anoop Korattikara, and Max Welling. Bayesian posterior sampling via stochastic gradient fisher scoring. *arXiv preprint arXiv:1206.6380*, 2012.

Dario Amodei, Sundaram Ananthanarayanan, Rishita Anubhai, Jingliang Bai, Eric Battenberg, Carl Case, Jared Casper, Bryan Catanzaro, Qiang Cheng, Guoliang Chen, et al. Deep speech 2: End-to-end speech recognition in english and mandarin. In *International conference on machine learning*, pages 173–182. PMLR, 2016.

Olivier Bachem, Mario Lucic, and Andreas Krause. Coresets for nonparametric estimation-the case of dp-means. In *International Conference on Machine Learning*, pages 209–217. PMLR, 2015.

Olivier Bachem, Mario Lucic, S Hamed Hassani, and Andreas Krause. Approximate k-means++ in sublinear time. In *Proceedings of the AAAI conference on artificial intelligence*, volume 30, 2016.

Olivier Bachem, Mario Lucic, and Andreas Krause. Scalable k-means clustering via lightweight coresets. In *Proceedings of the 24th ACM SIGKDD International Conference on Knowledge Discovery & Data Mining*, pages 1119–1127, 2018.

Rémi Bardenet, Arnaud Doucet, and Chris Holmes. Towards scaling up markov chain monte carlo: an adaptive subsampling approach. In *International conference on machine learning*, pages 405–413. PMLR, 2014.

Rémi Bardenet, Arnaud Doucet, and Chris Holmes. On markov chain monte carlo methods for tall data. *Journal of Machine Learning Research*, 18(47), 2017.

Atilim Gunes Baydin, Barak A Pearlmutter, Alexey Andreyevich Radul, and Jeffrey Mark Siskind. Automatic differentiation in machine learning: a survey. *Journal of Marchine Learning Research*, 18:1–43, 2018.

Eden Belouadah and Adrian Popescu. Scail: Classifier weights scaling for class incremental learning. In *Proceedings of the IEEE/CVF winter conference on applications of computer vision*, pages 1266–1275, 2020.

MJ Betancourt. The fundamental incompatibility of hamiltonian monte carlo and data subsampling. *arXiv preprint arXiv:1502.01510*, 2015.

Joris Bierkens, Paul Fearnhead, and Gareth Roberts. The zig-zag process and super-efficient sampling for bayesian analysis of big data. *The Annals of Statistics*, 47(3), jun 2019. doi: 10.1214/18-aos1715. URL `https://doi.org/10.1214%2F18-aos1715`.

Ondrej Bohdal, Yongxin Yang, and Timothy Hospedales. Flexible dataset distillation: Learn labels instead of images. *arXiv preprint arXiv:2006.08572*, 2020.

Glenn W Brier. Verification of forecasts expressed in terms of probability. *Monthly weather review*, 78(1):1–3, 1950.

Trevor Campbell and Boyan Beronov. Sparse variational inference: Bayesian coresets from scratch. *Advances in Neural Information Processing Systems*, 32, 2019.

Trevor Campbell and Tamara Broderick. Bayesian coreset construction via greedy iterative geodesic ascent. In *International Conference on Machine Learning*, pages 698–706. PMLR, 2018.

Trevor Campbell and Tamara Broderick. Automated scalable bayesian inference via hilbert coresets. *The Journal of Machine Learning Research*, 20(1):551–588, 2019.

Francisco M Castro, Manuel J Marín-Jiménez, Nicolás Guil, Cordelia Schmid, and Karteek Alahari. End-to-end incremental learning. In *Proceedings of the European conference on computer vision (ECCV)*, pages 233–248, 2018.

Rodolfo C Cavalcante, Rodrigo C Brasileiro, Victor LF Souza, Jarley P Nobrega, and Adriano LI Oliveira. Computational intelligence and financial markets: A survey and future directions. *Expert Systems with Applications*, 55:194–211, 2016.

George Cazenavette, Tongzhou Wang, Antonio Torralba, Alexei A Efros, and Jun-Yan Zhu. Dataset distillation by matching training trajectories. In *Proceedings of the IEEE/CVF Conference on Computer Vision and Pattern Recognition*, pages 4750–4759, 2022.

George Cazenavette, Tongzhou Wang, Antonio Torralba, Alexei A Efros, and Jun-Yan Zhu. Generalizing dataset distillation via deep generative prior. *Proceedings of the IEEE/CVF conference on computer vision and pattern recognition*, 2023.

Naitong Chen, Zuheng Xu, and Trevor Campbell. Bayesian inference via sparse hamiltonian flows. *Advances in Neural Information Processing Systems*, 35:20876–20888, 2022.

Tianqi Chen, Emily Fox, and Carlos Guestrin. Stochastic gradient hamiltonian monte carlo. In *International conference on machine learning*, pages 1683–1691. PMLR, 2014.

Yutian Chen, Max Welling, and Alex Smola. Super-samples from kernel herding. *arXiv preprint arXiv:1203.3472*, 2012.

Francesco Croce, Maksym Andriushchenko, Vikash Sehwag, Edoardo Debenedetti, Nicolas Flammarion, Mung Chiang, Prateek Mittal, and Matthias Hein. Robustbench: a standardized adversarial robustness benchmark. In *Thirty-fifth Conference on Neural Information Processing Systems Datasets and Benchmarks Track (Round 2)*, 2021. URL `https://openreview.net/forum?id=SSKZPJCt7B`.

Justin Cui, Ruochen Wang, Si Si, and Cho-Jui Hsieh. DC-BENCH: Dataset condensation benchmark. In *Thirty-sixth Conference on Neural Information Processing Systems Datasets and Benchmarks Track*, 2022. URL `https://openreview.net/forum?id=Bs8iFQ7AM6`.

Zhiwei Deng and Olga Russakovsky. Remember the past: Distilling datasets into addressable memories for neural networks. *arXiv preprint arXiv:2206.02916*, 2022.

Jacob Devlin, Ming-Wei Chang, Kenton Lee, and Kristina Toutanova. Bert: Pre-training of deep bidirectional transformers for language understanding. *arXiv preprint arXiv:1810.04805*, 2018.

Alexey Dosovitskiy, Lucas Beyer, Alexander Kolesnikov, Dirk Weissenborn, Xiaohua Zhai, Thomas Unterthiner, Mostafa Dehghani, Matthias Minderer, Georg Heigold, Sylvain Gelly, et al. An image is worth 16x16 words: Transformers for image recognition at scale. *arXiv preprint arXiv:2010.11929*, 2020.

Jiawei Du, Yidi Jiang, Vincent TF Tan, Joey Tianyi Zhou, and Haizhou Li. Minimizing the accumulated trajectory error to improve dataset distillation. *Proceedings of the IEEE/CVF conference on computer vision and pattern recognition*, 2023.

Reza Zanjirani Farahani and Masoud Hekmatfar. *Facility location: concepts, models, algorithms and case studies*. Springer Science & Business Media, 2009.

Dan Feldman and Michael Langberg. A unified framework for approximating and clustering data. In *Proceedings of the forty-third annual ACM symposium on Theory of computing*, pages 569–578, 2011.

Dan Feldman, Matthew Faulkner, and Andreas Krause. Scalable training of mixture models via coresets. *Advances in neural information processing systems*, 24, 2011.

Dan Feldman, Melanie Schmidt, and Christian Sohler. Turning big data into tiny data: Constant-size coresets for k-means, pca, and projective clustering. *SIAM Journal on Computing*, 49(3):601–657, 2020.

Marguerite Frank, Philip Wolfe, et al. An algorithm for quadratic programming. *Naval research logistics quarterly*, 3(1-2):95–110, 1956.

Jakob Gawlikowski, Cedrique Rovile Njieutcheu Tassi, Mohsin Ali, Jongseok Lee, Matthias Humt, Jianxiang Feng, Anna Kruspe, Rudolph Triebel, Peter Jung, Ribana Roscher, et al. A survey of uncertainty in deep neural networks. *Artificial Intelligence Review*, pages 1–77, 2023.

Spyros Gidaris and Nikos Komodakis. Dynamic few-shot visual learning without forgetting. In *Proceedings of the IEEE conference on computer vision and pattern recognition*, pages 4367–4375, 2018.

Chengcheng Guo, Bo Zhao, and Yanbing Bai. Deepcore: A comprehensive library for coreset selection in deep learning. In *Database and Expert Systems Applications: 33rd International Conference, DEXA 2022, Vienna, Austria, August 22–24, 2022, Proceedings, Part I*, pages 181–195. Springer, 2022.

Kaiming He, Xiangyu Zhang, Shaoqing Ren, and Jian Sun. Deep residual learning for image recognition. In *Proceedings of the IEEE conference on computer vision and pattern recognition*, pages 770–778, 2016a.

Kaiming He, Xiangyu Zhang, Shaoqing Ren, and Jian Sun. Deep residual learning for image recognition. In *Proceedings of the IEEE conference on computer vision and pattern recognition*, pages 770–778, 2016b.

Dan Hendrycks and Thomas Dietterich. Benchmarking neural network robustness to common corruptions and perturbations. *arXiv preprint arXiv:1903.12261*, 2019.

Geoffrey E Hinton. Training products of experts by minimizing contrastive divergence. *Neural computation*, 14 (8):1771–1800, 2002.

Matthew D Hoffman, Andrew Gelman, et al. The no-u-turn sampler: adaptively setting path lengths in hamiltonian monte carlo. *J. Mach. Learn. Res.*, 15(1):1593–1623, 2014.

Jonathan Huggins, Trevor Campbell, and Tamara Broderick. Coresets for scalable bayesian logistic regression. *Advances in neural information processing systems*, 29, 2016.

Tommi S Jaakkola and Michael I Jordan. A variational approach to bayesian logistic regression models and their extensions. In *Sixth International Workshop on Artificial Intelligence and Statistics*, pages 283–294. PMLR, 1997.

Zixuan Jiang, Jiaqi Gu, Mingjie Liu, and David Z Pan. Delving into effective gradient matching for dataset condensation. *arXiv preprint arXiv:2208.00311*, 2022.

James E Johndrow, Natesh S Pillai, and Aaron Smith. No free lunch for approximate mcmc. *arXiv preprint arXiv:2010.12514*, 2020.

Michael I Jordan, Zoubin Ghahramani, Tommi S Jaakkola, and Lawrence K Saul. An introduction to variational methods for graphical models. *Learning in graphical models*, pages 105–161, 1998.

Michael I Jordan, Zoubin Ghahramani, Tommi S Jaakkola, and Lawrence K Saul. An introduction to variational methods for graphical models. *Machine learning*, 37: 183–233, 1999.

Laurent Valentin Jospin, Hamid Laga, Farid Boussaid, Wray Buntine, and Mohammed Bennamoun. Hands-on bayesian neural networks—a tutorial for deep learning users. *IEEE Computational Intelligence Magazine*, 17(2): 29–48, 2022.

HM Dipu Kabir, Abbas Khosravi, Mohammad Anwar Hosen, and Saeid Nahavandi. Neural network-based uncertainty quantification: A survey of methodologies and applications. *IEEE access*, 6:36218–36234, 2018.

Justin Ker, Lipo Wang, Jai Rao, and Tchoyoson Lim. Deep learning applications in medical image analysis. *Ieee Access*, 6:9375–9389, 2017.

Krishnateja Killamsetty, Sivasubramanian Durga, Ganesh Ramakrishnan, Abir De, and Rishabh Iyer. Grad-match: Gradient matching based data subset selection for efficient deep model training. In *International Conference on Machine Learning*, pages 5464–5474. PMLR, 2021a.

Krishnateja Killamsetty, Durga Sivasubramanian, Ganesh Ramakrishnan, and Rishabh Iyer. Glister: Generalization based data subset selection for efficient and robust learning. In *Proceedings of the AAAI Conference on Artificial Intelligence*, volume 35, pages 8110–8118, 2021b.

Balhae Kim, Jungwon Choi, Seanie Lee, Yoonho Lee, Jung-Woo Ha, and Juho Lee. On divergence measures for bayesian pseudocoresets. *arXiv preprint arXiv:2210.06205*, 2022a.

Jang-Hyun Kim, Jinuk Kim, Seong Joon Oh, Sangdoo Yun, Hwanjun Song, Joonhyun Jeong, Jung-Woo Ha, and Hyun Oh Song. Dataset condensation via efficient synthetic-data parameterization. In *International Conference on Machine Learning*, pages 11102–11118. PMLR, 2022b.

Anoop Korattikara, Yutian Chen, and Max Welling. Austerity in mcmc land: Cutting the metropolis-hastings budget. In *International conference on machine learning*, pages 181–189. PMLR, 2014.

Alex Krizhevsky and Geoffrey Hinton. Learning multiple layers of features from tiny images. Technical Report 0, University of Toronto, Toronto, Ontario, 2009. URL `https://www.cs.toronto.edu/~kriz/learning-features-2009-TR.pdf`.

Alex Krizhevsky, Ilya Sutskever, and Geoffrey E Hinton. Imagenet classification with deep convolutional neural networks. *Communications of the ACM*, 60(6):84–90, 2017a.

Alex Krizhevsky, Ilya Sutskever, and Geoffrey E Hinton. Imagenet classification with deep convolutional neural networks. *Communications of the ACM*, 60(6):84–90, 2017b.

Alp Kucukelbir, Dustin Tran, Rajesh Ranganath, Andrew Gelman, and David M Blei. Automatic differentiation variational inference. *Journal of machine learning research*, 2017.

Ya Le and Xuan Yang. Tiny imagenet visual recognition challenge. *CS 231N*, 7(7):3, 2015.

Yann LeCun, Léon Bottou, Yoshua Bengio, and Patrick Haffner. Gradient-based learning applied to document recognition. *Proceedings of the IEEE*, 86(11):2278–2324, 1998.

Saehyung Lee, Sanghyuk Chun, Sangwon Jung, Sangdoo Yun, and Sungroh Yoon. Dataset condensation with contrastive signals. In *International Conference on Machine Learning*, pages 12352–12364. PMLR, 2022.

Guang Li, Ren Togo, Takahiro Ogawa, and Miki Haseyama. Dataset distillation using parameter pruning. *arXiv preprint arXiv:2209.14609*, 2022.

Yanqing Liu, Jianyang Gu, Kai Wang, Zheng Zhu, Wei Jiang, and Yang You. Dream: Efficient dataset distillation by representative matching. *arXiv preprint arXiv:2302.14416*, 2023.

Noel Loo, Ramin Hasani, Alexander Amini, and Daniela Rus. Efficient dataset distillation using random feature approximation. *arXiv preprint arXiv:2210.12067*, 2022.

Dougal Maclaurin and Ryan P Adams. Firefly monte carlo: Exact mcmc with subsets of data. *arXiv preprint arXiv:1403.5693*, 2014.

Dionysis Manousakas, Zuheng Xu, Cecilia Mascolo, and Trevor Campbell. Bayesian pseudocoresets. *Advances in Neural Information Processing Systems*, 33:14950–14960, 2020.

Baharan Mirzasoleiman, Jeff Bilmes, and Jure Leskovec. Coresets for data-efficient training of machine learning models. In *International Conference on Machine Learning*, pages 6950–6960. PMLR, 2020.

Mahdi Pakdaman Naeini, Gregory Cooper, and Milos Hauskrecht. Obtaining well calibrated probabilities using bayesian binning. In *Proceedings of the AAAI conference on artificial intelligence*, volume 29, 2015.

Tigran Nagapetyan, Andrew B Duncan, Leonard Hasenclever, Sebastian J Vollmer, Lukasz Szpruch, and Konstantinos Zygalakis. The true cost of stochastic gradient langevin dynamics. *arXiv preprint arXiv:1706.02692*, 2017.

Cian Naik, Judith Rousseau, and Trevor Campbell. Fast bayesian coresets via subsampling and quasi-newton refinement. *Advances in Neural Information Processing Systems*, 35:70–83, 2022.

Radford M Neal, S Brooks, A Gelman, G Jones, XL Meng, et al. Handbook of markov chain monte carlo. *Press C, editor*, 22011, 2011a.

Radford M Neal et al. Mcmc using hamiltonian dynamics. *Handbook of markov chain monte carlo*, 2(11):2, 2011b.

Timothy Nguyen, Zhourong Chen, and Jaehoon Lee. Dataset meta-learning from kernel ridge-regression. In *International Conference on Learning Representations*, 2021. URL `https://openreview.net/forum?id=l-PrrQrK0QR`.

Murray Pollock, Paul Fearnhead, Adam M Johansen, and Gareth O Roberts. Quasi-stationary monte carlo and the scale algorithm. *Journal of the Royal Statistical Society Series B: Statistical Methodology*, 82(5):1167–1221, 2020.

Alec Radford, Jong Wook Kim, Chris Hallacy, Aditya Ramesh, Gabriel Goh, Sandhini Agarwal, Girish Sastry, Amanda Askell, Pamela Mishkin, Jack Clark, et al. Learning transferable visual models from natural language supervision. In *International conference on machine learning*, pages 8748–8763. PMLR, 2021.

Rajesh Ranganath, Sean Gerrish, and David Blei. Black box variational inference. In *Artificial intelligence and statistics*, pages 814–822. PMLR, 2014.

Sylvestre-Alvise Rebuffi, Alexander Kolesnikov, Georg Sperl, and Christoph H Lampert. icarl: Incremental classifier and representation learning. In *Proceedings of the IEEE conference on Computer Vision and Pattern Recognition*, pages 2001–2010, 2017.

Hippolyt Ritter, Aleksandar Botev, and David Barber. A scalable laplace approximation for neural networks. In *6th international conference on learning representations, ICLR 2018-conference track proceedings*, volume 6. International Conference on Representation Learning, 2018.

Christian Robert and George Casella. A short history of markov chain monte carlo: Subjective recollections from incomplete data. *Statistical Science*, 26(1), feb 2011. doi: 10.1214/10-sts351. URL `https://doi.org/10.1214%2F10-sts351`.

Christian P Robert, George Casella, and George Casella. *Monte Carlo statistical methods*, volume 2. Springer, 1999.

Ozan Sener and Silvio Savarese. Active learning for convolutional neural networks: A core-set approach. *arXiv preprint arXiv:1708.00489*, 2017.

Pierre Sermanet, Soumith Chintala, and Yann LeCun. Convolutional neural networks applied to house numbers digit classification. In *Proceedings of the 21st international conference on pattern recognition (ICPR2012)*, pages 3288–3291. IEEE, 2012.

Karen Simonyan and Andrew Zisserman. Very deep convolutional networks for large-scale image recognition. *arXiv preprint arXiv:1409.1556*, 2014.

Christian Szegedy, Wojciech Zaremba, Ilya Sutskever, Joan Bruna, Dumitru Erhan, Ian Goodfellow, and Rob Fergus. Intriguing properties of neural networks. *arXiv preprint arXiv:1312.6199*, 2013.

Yee Whye Teh, Max Welling, Simon Osindero, and Geoffrey E Hinton. Energy-based models for sparse overcomplete representations. *Journal of Machine Learning Research*, 4(Dec):1235–1260, 2003.

Mariya Toneva, Alessandro Sordoni, Remi Tachet des Combes, Adam Trischler, Yoshua Bengio, and Geoffrey J Gordon. An empirical study of example forgetting during deep neural network learning. *arXiv preprint arXiv:1812.05159*, 2018.

Martin J Wainwright, Michael I Jordan, et al. Graphical models, exponential families, and variational inference. *Foundations and Trends® in Machine Learning*, 1(1–2): 1–305, 2008.

Kai Wang, Bo Zhao, Xiangyu Peng, Zheng Zhu, Shuo Yang, Shuo Wang, Guan Huang, Hakan Bilen, Xinchao Wang, and Yang You. Cafe: Learning to condense dataset by aligning features. In *Proceedings of the IEEE/CVF Conference on Computer Vision and Pattern Recognition*, pages 12196–12205, 2022.

Tongzhou Wang, Jun-Yan Zhu, Antonio Torralba, and Alexei A Efros. Dataset distillation. *arXiv preprint arXiv:1811.10959*, 2018.

Max Welling. Herding dynamical weights to learn. In *Proceedings of the 26th Annual International Conference on Machine Learning*, pages 1121–1128, 2009.

Max Welling and Yee W Teh. Bayesian learning via stochastic gradient langevin dynamics. In *Proceedings of the 28th international conference on machine learning (ICML-11)*, pages 681–688. Citeseer, 2011.

Han Xiao, Kashif Rasul, and Roland Vollgraf. Fashion-mnist: a novel image dataset for benchmarking machine learning algorithms. *arXiv preprint arXiv:1708.07747*, 2017.

Ruonan Yu, Songhua Liu, and Xinchao Wang. Dataset distillation: A comprehensive review. *arXiv preprint arXiv:2301.07014*, 2023.

Jacky Zhang, Rajiv Khanna, Anastasios Kyrillidis, and Sanmi Koyejo. Bayesian coresets: Revisiting the nonconvex optimization perspective. In *International Conference on Artificial Intelligence and Statistics*, pages 2782–2790. PMLR, 2021.

Lei Zhang, Jie Zhang, Bowen Lei, Subhabrata Mukherjee, Xiang Pan, Bo Zhao, Caiwen Ding, Yao Li, and Dongkuan Xu. Accelerating dataset distillation via model augmentation. *Proceedings of the IEEE/CVF conference on computer vision and pattern recognition*, 2023.

Bo Zhao and Hakan Bilen. Dataset condensation with differentiable siamese augmentation. In *International Conference on Machine Learning*, pages 12674–12685. PMLR, 2021.

Bo Zhao and Hakan Bilen. Synthesizing informative training samples with gan. *arXiv preprint arXiv:2204.07513*, 2022.

Bo Zhao and Hakan Bilen. Dataset condensation with distribution matching. In *Proceedings of the IEEE/CVF Winter Conference on Applications of Computer Vision*, pages 6514–6523, 2023.

Bo Zhao, Konda Reddy Mopuri, and Hakan Bilen. Dataset condensation with gradient matching. In *International Conference on Learning Representations*, 2021. URL `https://openreview.net/forum?id=mSAKhLYLSsl`.

Ganlong Zhao, Guanbin Li, Yipeng Qin, and Yizhou Yu. Improved distribution matching for dataset condensation. In *Proceedings of the IEEE/CVF conference on computer vision and pattern recognition*, 2023.

Yongchao Zhou, Ehsan Nezhadarya, and Jimmy Ba. Dataset distillation using neural feature regression. In Alice H. Oh, Alekh Agarwal, Danielle Belgrave, and Kyunghyun Cho, editors, *Advances in Neural Information Processing Systems*, 2022. URL `https://openreview.net/forum?id=2clwrA2tfik`.

Bayesian Pseudo-Coresets via Contrastive Divergence (Supplementary Material)

Piyush Tiwary[1] **Kumar Shubham**[1] **Vivek V. Kashyap**[1] **Prathosh A.P.**[1]

[1]Department of Electrical Communuication Engineering,

Indian Institute of Science, Bengaluru, Karnataka 560012, India

A TRAINING DETAILS AND HYPER PARAMETERS

In this section, we provide the implementation details of the proposed method. Our implementation can be found https://github.com/backpropagator/BPC-CD. During the training process, we randomly initialize the synthetic dataset using samples from the original training set. The overall cardinality of these synthetic sets is determined by the number of images considered for every class (ipc). For our experiments, we have considered ipc values of 1, 10 and 50. Furthermore, similar to previous works Kim et al. [2022a], Cazenavette et al. [2022], we have used Differentiable Siamese Augmentation (DSA) [Zhao and Bilen, 2021] strategies to enhance the performance of our model. DSA strategies include random crop, random flip, random brightness, random scale, and rotation. At any instant, we apply one of these augmentations to train our network. These augmentation techniques ensure that the model does not overfit on the given synthetic set and generates optimal parameters. DSA is applied to the synthetic set while running langevin dynamics and calculating the contrastive-divergence-based loss function.

We have also conducted additional experiments to evaluate the effectiveness of our method and other BPC baselines in the absence of DSA. The findings of the experiment are reported in Table 9. The results clearly indicate that the DSA has a positive impact on the performance of all BPC methods, which align with the observation made by Cui et al. [2022]. Nevertheless, even without the DSA-based augmentation strategy, our method outperforms other BPC baselines for 1 ipc.

As for the network used to calculate the energy, we take inspiration from previous works [Kim et al., 2022a, Wang et al., 2018, Lee et al., 2022, Cazenavette et al., 2022] and use a ConvNet architecture [Gidaris and Komodakis, 2018]. This architecture consists of multiple blocks of convolutional layer with filter dimension of 3×3 and channel size of 128. The network uses instance normalization, maxpool layer with stride 2, and RELU activation. In our experiments, we have used an architecture with three such blocks of convolution layers.

Next, we create a buffer of trajectories to sample parameters from the posterior of the original dataset. For this, we generate 100 different trajectories, each with 50 epochs trained using SGD optimizer with a batch size of 256 on the original training set. These parameters are used to obtain the gaussian variational approximation to estimate the loss function. Further, we use diagonal covariance matrix with diagonal entry of 0.001 for the re-parameterization trick used in gaussian approximation.

The pseudocode of the implementation is presented in Algorithm 1. The hyperparameters used are as follows: $P = 2000$, $\lambda = 0.01$, $n = 50$, $L = 100$, $\Sigma_{\mathbf{x}}^{1/2} = 0.001I$. These hyper-parameters are fixed across all the datasets. Further, we observe that there γ that can be fine-tuned for marginal improvements in performance. Specifically, γ is varied between $\{1, 10, 100, 1000\}$. Note that, we use same set of parameter to sample parameters during inference. All the experiments are conducted on a single NVIDIA RTX A6000 GPUs with 48GB memory.

Table 9: Comparison of the proposed method against other BPC baselines without using DSA on CIFAR10 dataset.

BPC-rkl (sghmc)		**BPC-W (sghmc)**		**BPC-fkl (hmc)**		**BPC-fkl (sghmc)**		**Ours**	
ipc =1	ipc = 10	ipc =1	ipc = 10	ipc =1	ipc = 10	ipc =1	ipc = 10	ipc =1	ipc = 10
19.70 ± 1.06	36.41 ± 0.75	27.66 ± 0.8	39.61 ± 1.12	32.61 ± 1.50	38.12 ± 1.19	28.25 ± 0.92	$\mathbf{41.85 \pm 1.47}$	$\mathbf{34.94 \pm 0.72}$	41.02 ± 0.66

Algorithm 1 Proposed Algorithm

Input : Set of SGD trajectories obtained from original dataset (τ), Number of langevin steps (L) needed to sample parameter from $\pi_{\tilde{\mathbf{x}}}$, Langevin step size (λ), Step size to modify pseudo-coreset (γ), Number of epochs (P)

```
 1: Initialize pseudo-coreset ($\tilde{x}$) using samples from original dataset $x$.
 2: for step in [1... P] : do
 3:     Sample $\tau_i \sim \tau$
 4:     Sample $\theta_k^+ \sim \tau_i$ where $\theta_k^+$ are parameters associated with $k^{th}$ epoch for $i^{th}$ trajectory.
 5:     Let $\theta^+ = \theta_k^+ + \Sigma_{\mathbf{x}}^{1/2}\varepsilon_{\mathbf{x}}$, $\varepsilon \sim \mathcal{N}(0, I)$
 6:     Let $\theta_0^- = \theta^+$
 7:     for t in [0 .... L] : do
 8:         Calculate energy associated with $\tilde{\mathbf{x}}$ and parameter $\theta_t^-$ i.e. $E(\theta_t^-, \tilde{\mathbf{x}}))$
 9:         $\theta_{t+1}^- = \theta_t^- - \lambda(\nabla_\theta E(\theta_t^-, \tilde{\mathbf{x}})) + \eta,\ \eta \sim \mathcal{N}(0, I)$
10:     Let $\theta^- = \theta_L^-$
11:     Calculate $\mathcal{L} = E((\theta^+, \tilde{\mathbf{x}})) - E((\theta^-, \tilde{\mathbf{x}}))$
12:     $\tilde{\mathbf{x}} \leftarrow \tilde{\mathbf{x}} - \gamma \nabla_{\tilde{\mathbf{x}}} \mathcal{L}$
```

B EXPERIMENTAL SETUP

B.1 BASELINE SETUP

We primarily present the results for different BPC frameworks. The experiment of Table 1 in the main manuscript uses the original hyperparameters mentioned in the respective papers. In cases where hyperparameters were not explicitly specified, we employed the default hyperparameters of CIFAR10. We have presented the results for BPC methods with only 1 and 10 ipc for the CIFAR100 and T-ImageNet datasets. We could not report the result for other scenarios due to the computational limitations. These methods demand a significant amount of GPU memory, which we currently lack, making it impractical to compute the desired results.

B.2 GPU AND TIME CONSUMPTION

We assess the computational efficiency of our method relative to other baselines by comparing the GPU memory consumption and the training time required to generate the pseudo-coresets for a single iteration. The findings of our results are presented in Fig. 2, where the iteration time is calculated by taking the average of the total time for 100 different iterations.

As illustrated in Fig. 2, our method requires relatively less time compared to other BPC methods for low ipc values and outperforms BPC-W for higher ipc values. Additionally, in our examination of GPU memory usage, we observe that BPC-W shows linear scaling in GPU memory consumption as the number of images per class increases. In contrast, our method maintains consistent memory usage across all ipc values. In our experiment, we found that our method utilizes only 37GB of memory, even for higher images per class. It's worth noting that other BPC baselines such as BPC-fKL and BPC-rKL are more memory-efficient than our method and deliver consistent performance across all the ipc values. We attribute this observation to the fact that BPC-fkl and BPC-rkl avoid MCMC sampling during training by making use of relevant approximations. Whereas, our method makes use of gradient-based MCMC sampling (langevin dynamics) for estimation of the objective function. For this reason, the GPU consumption of the proposed method is relatively higher than that of BPC-fkl and BPC-rkl.

Further, for a pseudo-coreset of size m, we run langevin-dynamics for k steps which leads to a complexity of $\mathcal{O}(km)$. Compared to inference on entire dataset of size n, the same would have a complexity of $\mathcal{O}(kn)$. Since $m \ll n$, pseudo-coresets are much more efficient for inference compared to full data. Since the pseudo-coreset size (m) is fixed during inference and only final value of each iteration is required in the consequent iteration of langevin dynamics, the memory complexity is just $\mathcal{O}(m)$. Again since $m \ll n$, pseudo-coresets are efficient in term of memory as well compared to full data inference.

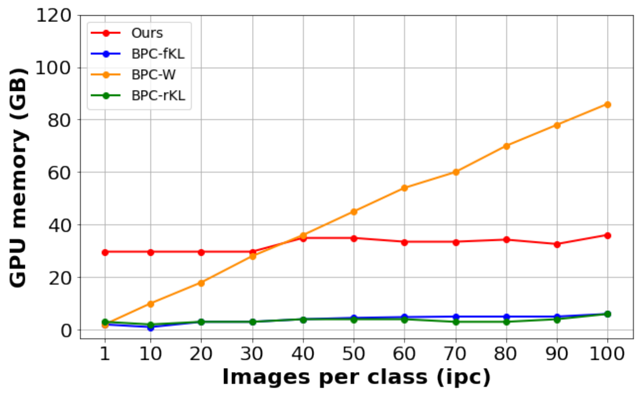

(a)

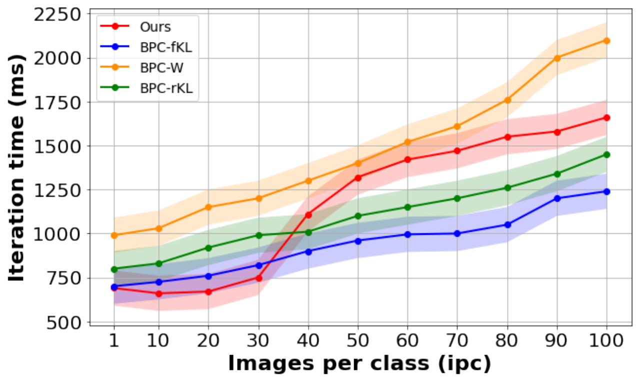

(b)

Figure 2: Computing GPU memory costs along with training time for different image per class.

C COMPARISON WITH CORESET METHODS

We have conducted a comparative analysis of our method with other coreset techniques such as Herding [Chen et al., 2012], K-Center [Sener and Savarese, 2017], and Forgetting [Toneva et al., 2018]. The outcomes of our experiments are listed in Table 10. The result clearly shows that our method outperforms other coreset techniques on all the dataset.

Table 10: Comparison of the proposed method with coreset baselines. The results are noted in form of (mean $\pm$ std. dev) where we have obtained test accuracy over five independent runs on the pseudo-coreset. The best performer across all methods is denoted in bold ($\boldsymbol{x \pm s}$). For ease of comparison, we color the second best performer with blue color.

	ipc	Ratio(%)	Herding	K-Center	Forgetting	Ours
MNIST	1	0.017	89.2 ± 1.6	89.3 ± 1.5	35.5 ± 5.6	$\mathbf{93.42 \pm 0.09}$
	10	0.17	93.7 ± 0.3	84.4 ± 1.7	68.1 ± 3.3	$\mathbf{97.71 \pm 0.24}$
	50	0.83	94.8 ± 0.2	97.4 ± 0.3	88.2 ± 1.2	$\mathbf{98.91 \pm 0.22}$
FMNIST	1	0.017	67.0 ± 1.9	66.9 ± 1.8	42.0 ± 5.5	$\mathbf{77.29 \pm 0.50}$
	10	0.17	71.1 ± 0.7	54.7 ± 1.5	53.9 ± 2.0	$\mathbf{88.40 \pm 0.21}$
	50	0.83	71.9 ± 0.8	68.3 ± 0.8	55.0 ± 1.1	$\mathbf{89.47 \pm 0.06}$
SVHN	1	0.014	20.9 ± 1.3	21.0 ± 1.5	12.1 ± 1.7	$\mathbf{66.74 \pm 0.09}$
	10	0.14	50.5 ± 3.3	14.0 ± 1.3	16.8 ± 1.2	$\mathbf{82.32 \pm 0.56}$
	50	0.7	72.6 ± 0.8	20.1 ± 1.4	27.2 ± 1.5	$\mathbf{88.41 \pm 0.12}$
Cifar10	1	0.02	21.5 ± 1.2	21.5 ± 1.3	13.5 ± 1.2	$\mathbf{46.87 \pm 0.20}$
	10	0.2	31.6 ± 0.7	14.7 ± 0.9	23.3 ± 1.0	$\mathbf{56.39 \pm 0.70}$
	50	1	23.3 ± 1.0	27.0 ± 1.4	23.3 ± 1.1	$\mathbf{71.93 \pm 0.17}$
Cifar100	1	0.2	8.4 ± 0.3	8.3 ± 0.3	4.5 ± 0.2	$\mathbf{23.97 \pm 0.11}$
	10	2	17.3 ± 0.3	7.1 ± 0.2	15.1 ± 0.3	$\mathbf{28.42 \pm 0.24}$
T-ImageNet	1	0.2	2.8 ± 0.2	3.03 ± 0.1	1.6 ± 0.1	$\mathbf{8.39 \pm 0.07}$
	10	2	6.3 ± 0.2	11.38 ± 0.1	5.1 ± 0.2	$\mathbf{17.82 \pm 0.39}$

D COMPARISON WITH DATASET CONDENSATION TECHNIQUES

We also compare our method with other data condensation (DC) techniques like Distillation (DD) [Wang et al., 2018], Flexible Dataset Distillation (LD) [Bohdal et al., 2020], Gradient Matching (DC) [Zhao et al., 2021], Differentiable Siamese Augmentation (DSA) [Zhao and Bilen, 2021], Distribution Matching (DM) [Zhao and Bilen, 2023], Neural Ridge Regression (KIP) [Nguyen et al., 2021], Condensed data to align features (CAFE) [Wang et al., 2022] and Matching Training Trajectories (MTT) [Cazenavette et al., 2022].

There are few fundamental differences between dataset condensation methods and BPC methods. We first enumerate these

Table 11: Efficiency comparison of the proposed method with several dataset condensation methods on CIFAR10.

ipc	GM GPU Memory (GB)	GM Time (s)	DSA GPU Memory (GB)	DSA Time (s)	MTT GPU Memory (GB)	MTT Time (s)	Ours GPU Memory (GB)	Ours Time (s)
1	38.88	0.4	43.09	0.3	44.82	1.2	**37.10**	**0.71**
10	42.78	11.4	46.06	7.5	50.98	12.7	**38.28**	**0.75**
50	46.39	32.9	53.20	24.4	68.10	26.8	**38.44**	**1.26**

Table 12: Comparison of the proposed method with dataset-condensation baselines. The results are noted in form of (mean $\pm$ std. dev) where we have obtained test accuracy over five independent runs on the pseudo-coreset. The best performer across all methods is denoted in bold ($\boldsymbol{x \pm s}$). For ease of comparison, we color the second best performer with blue color.

	Img/cls	Ratio%	DD	LD	GM	DSA	DM	CAFE	CAFE+DSA	KIP	MTT	Ours
MNIST	1	0.017	-	60.60 ± 2.86	92.01 ± 0.25	87.60 ± 0.07	88.89 ± 0.57	93.10 ± 0.30	90.80 ± 0.50	85.46 ± 0.04	89.85 ± 0.01	$\mathbf{93.42 \pm 0.09}$
	10	0.17	79.71 ± 8.3	87.05 ± 0.50	97.58 ± 0.10	97.39 ± 0.06	96.58 ± 0.11	97.20 ± 0.20	97.50 ± 0.10	97.15 ± 0.11	97.70 ± 0.02	$\mathbf{97.71 \pm 0.24}$
	50	0.83	-	93.30 ± 0.30	98.81 ± 0.03	98.97 ± 0.04	98.22 ± 0.05	98.60 ± 0.20	98.90 ± 0.20	98.36 ± 0.08	98.6 ± 0.01	$\mathbf{98.91 \pm 0.22}$
FMNIST	1	0.017	-	-	70.83 ± 0.01	70.45 ± 0.57	71.92 ± 0.70	77.10 ± 0.90	73.70 ± 0.70	-	77.14 ± 0.01	$\mathbf{77.29 \pm 0.50}$
	10	0.17	-	-	81.93 ± 0.07	84.70 ± 0.11	83.25 ± 0.09	83.00 ± 0.40	83.00 ± 0.30	-	$\mathbf{88.76 \pm 0.01}$	88.40 ± 0.21
	50	0.83	-	-	83.26 ± 0.17	88.55 ± 0.56	87.65 ± 0.03	84.80 ± 0.40	88.20 ± 0.30	-	89.33 ± 0.15	$\mathbf{89.47 \pm 0.06}$
SVHN	1	0.014	-	-	30.49 ± 0.57	31.18 ± 0.43	19.25 ± 1.39	42.60 ± 3.30	42.90 ± 3.01	-	57.55 ± 0.02	$\mathbf{66.74 \pm 0.09}$
	10	0.14	-	-	75.10 ± 0.40	78.39 ± 0.3	71.42 ± 1.01	75.90 ± 0.60	77.90 ± 0.60	-	72.56 ± 0.01	$\mathbf{82.32 \pm 0.56}$
	50	0.7	-	-	81.70 ± 0.14	82.50 ± 0.34	82.41 ± 0.52	81.30 ± 0.30	82.30 ± 0.40	-	83.73 ± 0.33	$\mathbf{88.41 \pm 0.12}$
CIFAR10	1	0.02	-	25.38 ± 0.2	28.10 ± 0.56	29.01 ± 0.64	26.40 ± 0.42	30.30 ± 1.10	31.60 ± 0.80	40.50 ± 0.40	46.08 ± 0.80	$\mathbf{46.87 \pm 0.2}$
	10	0.2	39.14 ± 2.30	37.50 ± 0.60	44.14 ± 0.60	51.85 ± 0.43	48.66 ± 0.03	46.30 ± 0.60	50.90 ± 0.50	53.10 ± 0.50	$\mathbf{64.27 \pm 0.80}$	56.39 ± 0.70
	50	1	-	41.70 ± 0.50	53.73 ± 0.44	60.77 ± 0.45	62.70 ± 0.07	55.50 ± 0.60	63.30 ± 0.40	58.60 ± 0.40	71.26 ± 0.50	$\mathbf{71.93 \pm 0.17}$
CIFAR100	1	0.2	-	11.50 ± 0.40	12.65 ± 0.32	13.88 ± 0.29	11.35 ± 0.18	12.04 ± 0.01	12.90 ± 0.30	14.01 ± 0.30	23.62 ± 0.63	$\mathbf{23.97 \pm 0.11}$
	10	2	-	-	25.28 ± 0.29	32.34 ± 0.40	29.38 ± 0.26	29.04 ± 0.01	27.80 ± 0.30	31.50 ± 0.20	$\mathbf{36.96 \pm 0.15}$	28.42 ± 0.24
T-ImageNet	1	0.2	-	-	5.27 ± 0.01	5.67 ± 0.01	3.82 ± 0.01	-	-	-	8.27 ± 0.01	$\mathbf{8.39 \pm 0.07}$
	10	2	-	-	12.83 ± 0.01	16.43 ± 0.02	13.51 ± 0.01	-	-	-	$\mathbf{20.11 \pm 0.02}$	17.82 ± 0.39

differences here for clarity:

1. **Objective function**: One of the key differences between Dataset Condensation (DC) and BPC is the underlying formulation and the loss objective. Dataset condensation methods mostly rely on heurist objective function to '**match the performance**' of synthetic data and original data; where the measure of performance matching varies for different methods. For e.g., GM [Zhao et al., 2021] relies on matching the gradient direction of a model trained on synthetic data with a model trained on the original data; similarly, MTT [Cazenavette et al., 2022] relies on matching SGD trajectories of the synthetic data and original data. Hence, these methods don't have a principled way of coming up with loss objective. However, BPC methods on the other hand follow a single principle for loss objective - a divergence measure between true posterior and pseudo-coreset posterior, which is much more principled. Different BPC method opt for different divergence measure, in context of our work, we choose to work with contrastive divergence for the reasons outlined in the paper.
2. **Bayesian v/s Non-Bayesian**: Another fundamental difference between the two domains is that BPC methods are purely bayesian, particularly, they treat parameters of the network as random variable and work on matching the distribution of this random variable via divergence minimization. On the other hand, DC methods are non-bayesian and work with point estimates of models.
3. **Optimization Strategy**: Finally, the pivotal difference between BPC methods and DC methods, that makes the former more efficient is the optimization strategy employed. Since DC methods rely on 'performance matching', it is inadvertent to train a model on synthetic and original data, then match the performance using appropriate metric. To learn the synthetic data in this case, one has to backpropagate the gradients through the model training steps as well. This would require computation of second-order derivatives. This is what we refer to as bi-level optimization. However, in case of BPC methods like ours, there is no such need of higher order derivatives. This is because we don't use bi-level optimization for BPC construction. This difference in optimization strategy makes BPC much more efficient in practice. The quantitative results to illustrate this claim can be found in Table 11, where we compare the GPU memory consumed and time taken for every iteration by different methods. It can be seen that dataset condensation consume significant memory and time.

The performance comparison results are shown in Table 12. We find that the performance of our method is better than almost all the DC baselines, whereas MTT stands out to be a close second in most of the cases. This shows that our method, although falling under the category of Bayesian pseudo-coreset, achieves a performance that is comparable to that of heuristic DC methods. It is to be noted that the DC methods are not the direct competitors of our method. However, we have shown that

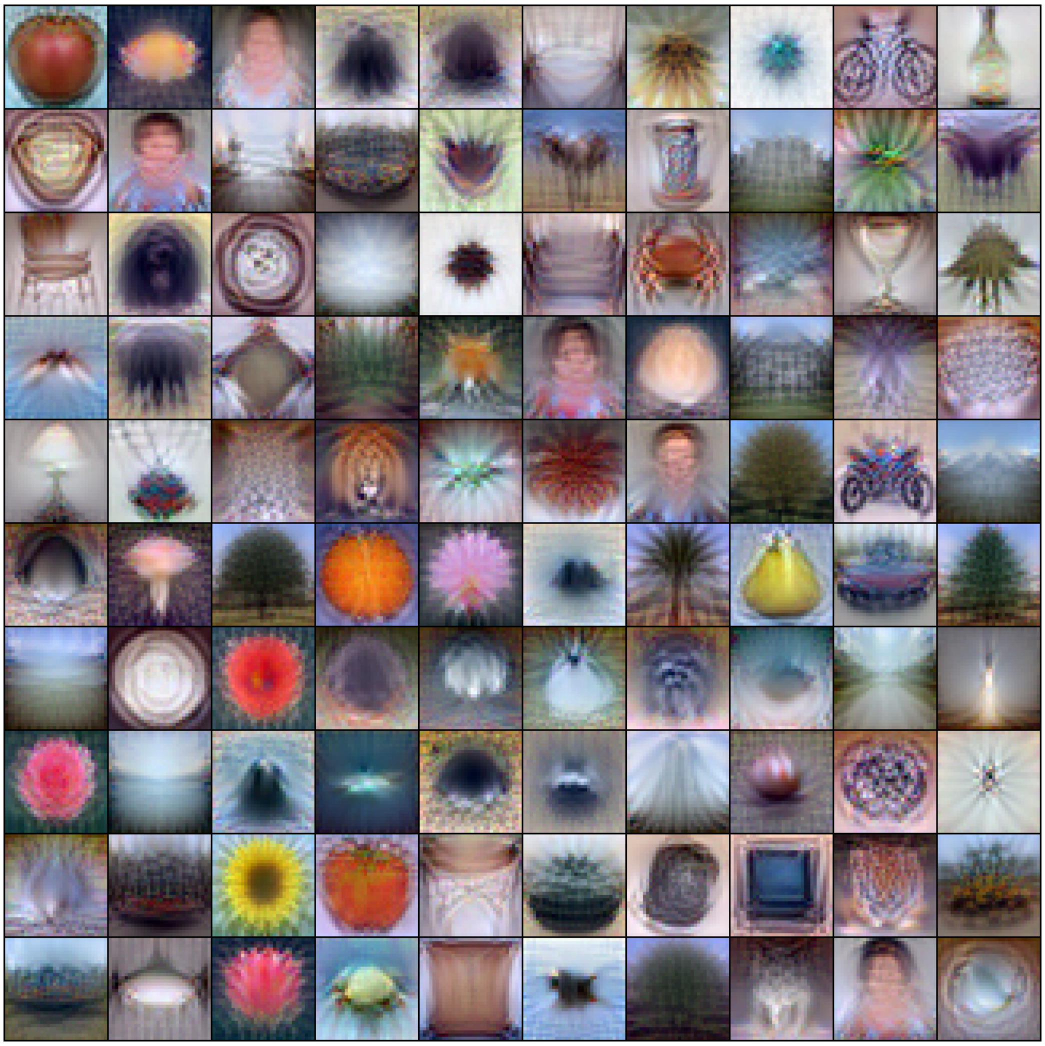

Figure 3: Visualizations of pseudo-coresets for CIFAR100 with 1 ipc.

our method, although a BPC, surpasses (or comes very close to) the SoTA DC methods such as MTT [Cazenavette et al., 2022].

E VISUALIZATIONS FOR CIFAR100 AND TINY-IMAGENET

In this section, we present the visualizations for pseudo-coresets of large datasets like CIFAR100 and Tiny-Imagenet datasets. We present generated synthetic images for both 1 and 10 images per class. We provide the visualization for 1 image per class on both datasets in Fig. 3 and Fig. 4, respectively. Fig. 5a and Fig. 5b include visualization for CIFAR100 datasets with 10 ipc wherein each image is divided based on the number of classes. Similarly, we split the image into 50 classes for the Tiny-ImageNet dataset for 10 ipc in Fig. 6 and Fig. 7.

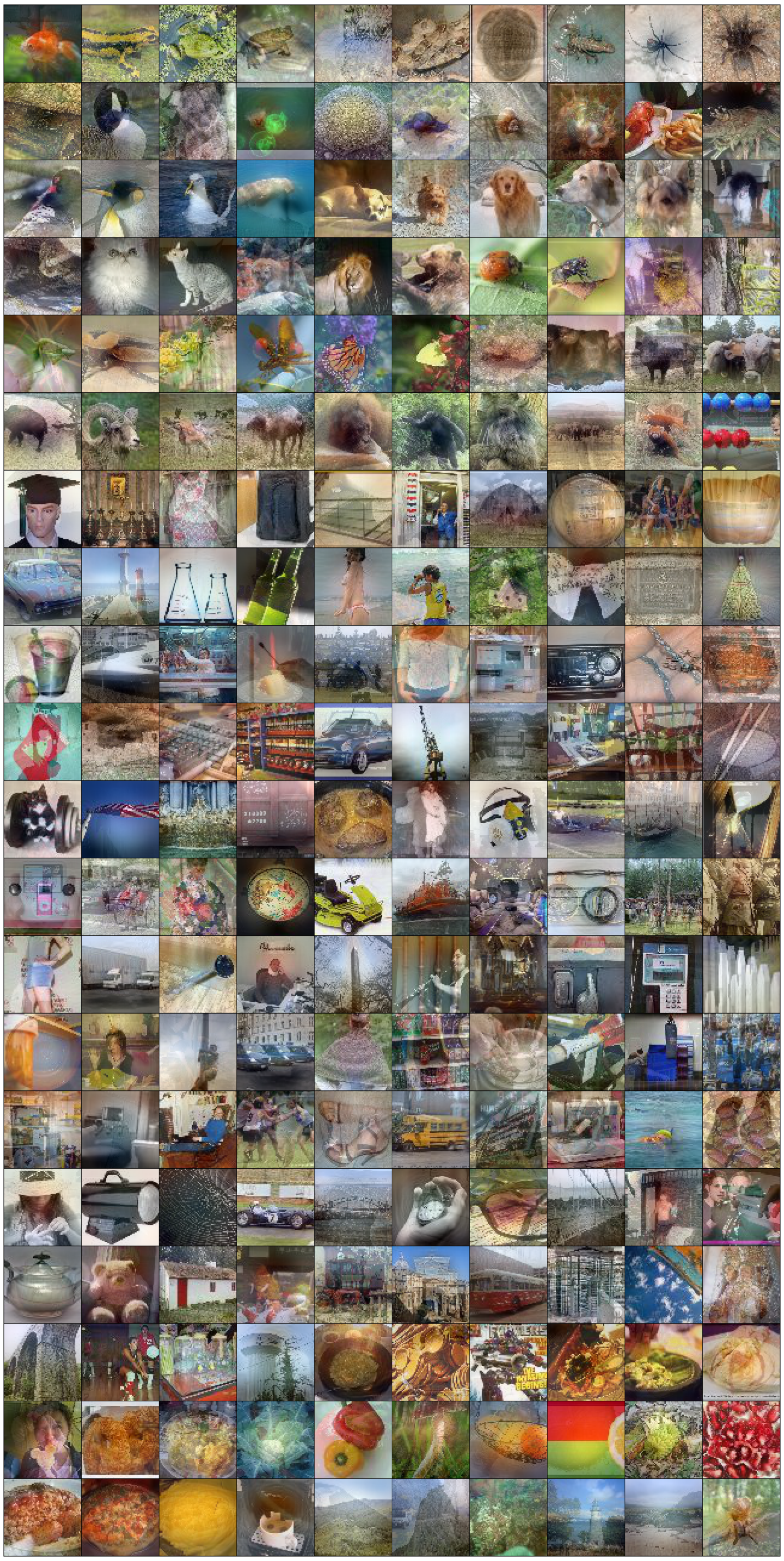
Figure 4: Visualizations of pseudo-coresets for Tiny ImageNet with 1 ipc.

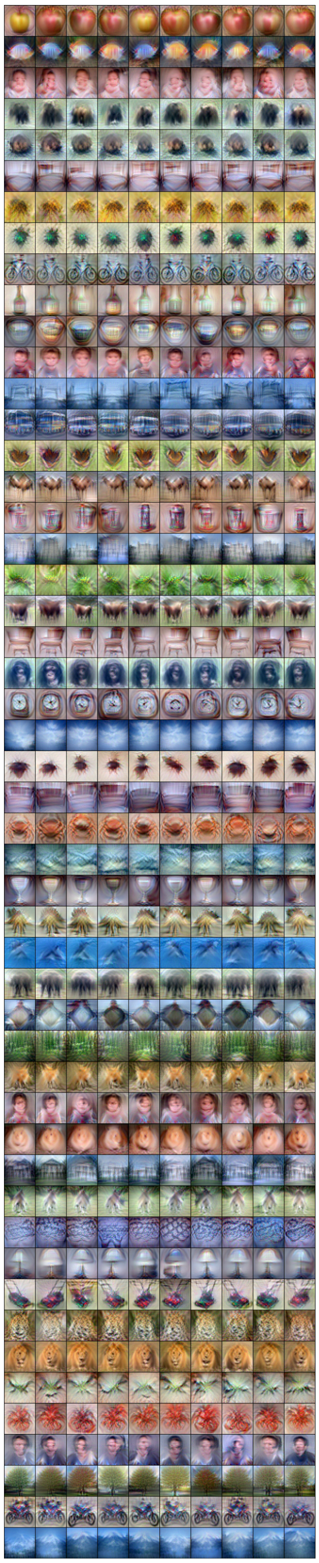
(a) Classes 0-50

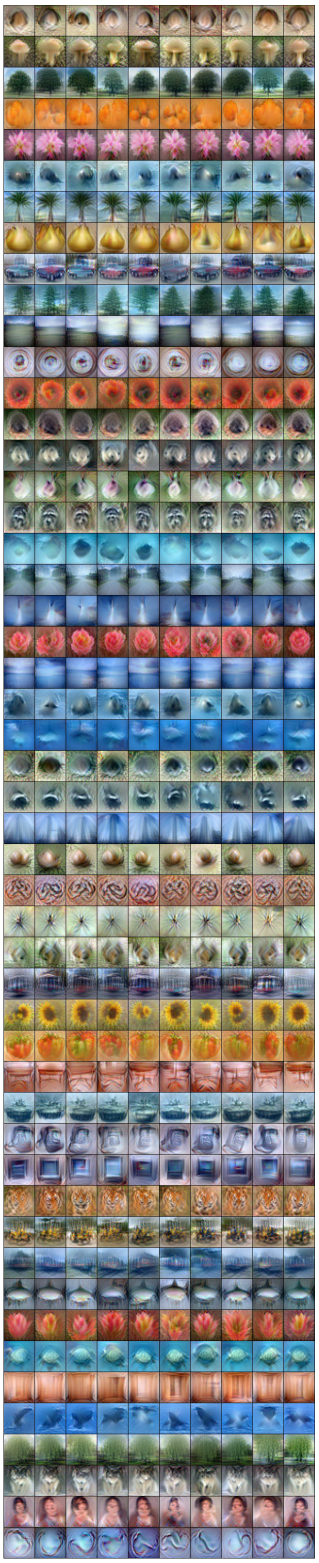
(b) Classes 50-100

Figure 5: Visualizations for pseudo-coresets for CIFAR100 with 10 ipc

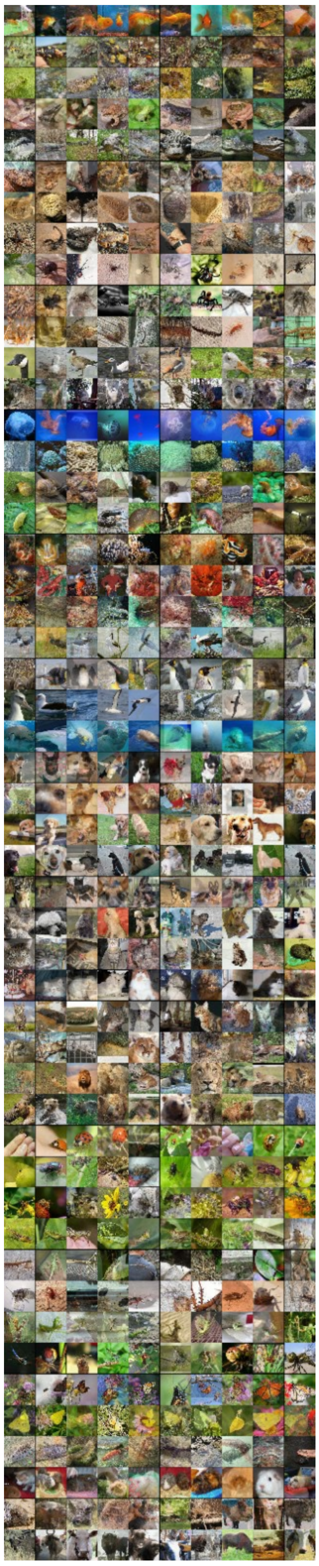
(a) Classes 0-50

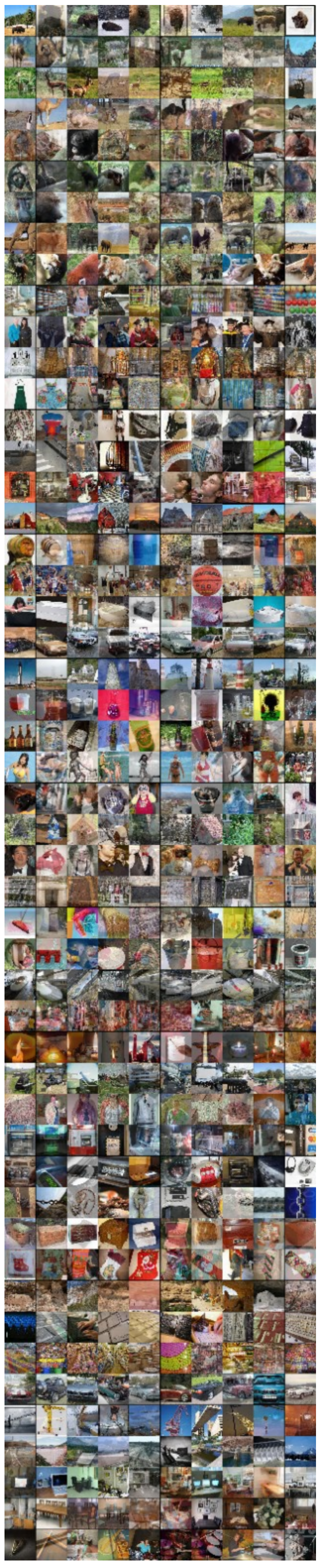
(b) Classes 50-100

Figure 6: Visualizations of psuedo-coresets for Tiny ImageNet with 10 ipc

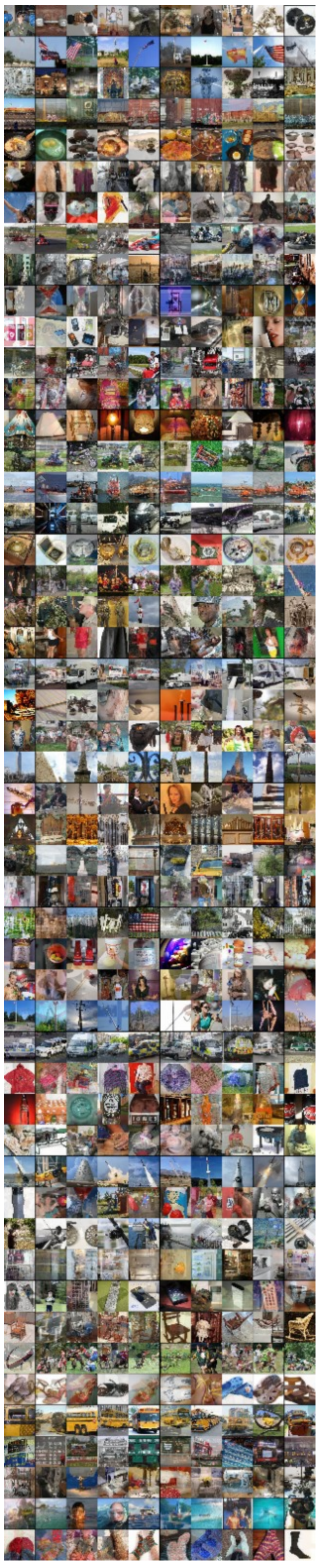
(a) Classes 100-150

(b) Classes 150-200

Figure 7: Visualizations of pseudo-coresets for Tiny ImageNet with 10 ipc